Chair of Hydrology

Albert-Ludwigs-University of Freiburg

Max Gregoire

Implementation of the stokes flow in the hydrological model RoGeR

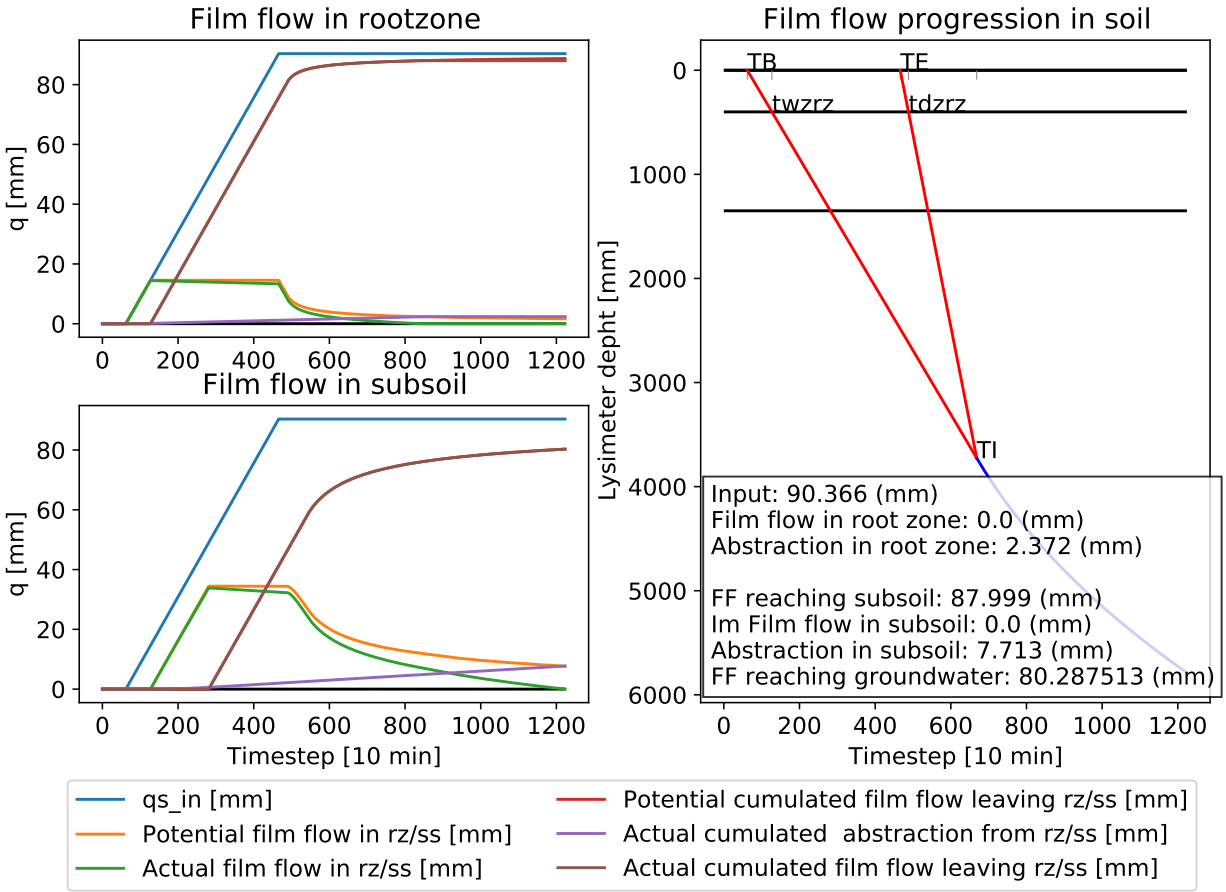

MSc-Thesis under the guidance of Prof. Dr. Markus Weiler

and M.Sc. Robin Schwemmle

Freiburg i. Br., January 2022

Chair of Hydrology

Albert-Ludwigs-University of Freiburg

Max Gregoire

Implementation of the stokes flow in the hydrological model RoGeR

Examiner: Prof. Dr. Markus Weiler

Co-Examiner: Prof. Dr. Kerstin Stahl

MSc-Thesis under the guidance of Prof. Dr. Markus Weiler
and M.Sc. Robin Schwemmle

Freiburg i. Br., January 2022

Declaration of Authorship

I hereby declare and confirm that this thesis is entirely the result of my own original work. Where other sources of information have been used, they have been indicated as such and properly acknowledged. I further declare that this or similar work has not been submitted for credit elsewhere.

Freiburg i. Br., 15 January 2021

Max Gregoire

Table of Contents

List of Figures

List of Tables

List of Abbreviations

HOF	Hortonian overland flow
IN3M	INfiltration–INitiation–INteraction
RoGeR	Runoff Generation Research
SOF	Saturated overland flow
SSF	Subsurface flow
WCW	water content wave

List of Symbols

η	Kineamtic viscosity	L^2T^{-1}
Ψ	Wetting front suction	L
$\theta_{d_{rel}}$	Relative soil moisture deficit	-
θ_{init}	Inital volumetric water content	-
θ_{lo}	Initial volumetric water content	-
θ_{out}	Volumetric water content after the water content wave	-
θ_{pwp}	Volumetric water content at permanent welting point	-
θ_{sat}	Saturated volumetric water content	-
θ_{up}	Maximum volumetric water content	-
a	Velocity-modulation coefficent	-
b	Exponent of power law relationship	-
c	Drainage front velocity	LT^{-1}
dt	Time step	T
F	Film thickness	L
f	Fudge parameter	-
g	Acceleration of gravity	L^2T^{-1}
K_s	Saturated hydraulic conductivity	LT^{-1}
L	specific contact area	L^2L^{-3}
ptc	Parameter: percentage of termination criterion	-
q	Volume flux of the water film	LT^{-1}
q_s	Volume flux density at the soil surface	LT^{-1}
q_{end}	Volume flux densitiy for end criterion	LT^{-1}
T_B	Starting point of the input pulse	T
T_E	Starting point of the input pulse	T
T_I	Intersection time of wetting and drainage front	T
T_W	Arrival time of the wetting front	T
v	Wetting front velocity	LT^{-1}
V_{WCW}	Total volume of the WCW	L
w	Mobile water content	-
z_D	Depth of the drainage front	L

Z_I	Intersection depth of wetting and drainage front	L
z_W	Depth of the wetting front	L

Abstract

Preferential flow is a non-negligible process in the soil in terms of water distribution and solute transport. In the existing hydrological models, preferential flow is often tried to be included in the model as capillary flow in a dual-porosity approach. The stokes or viscous flow describes the preferential flow as a gravitationally driven film flow that can be modeled without many parameters. In this feasibility study, an attempt was made to integrate the stokes flow into the hydrological model RoGeR. The modeling of the abstraction from the film flow into the soil matrix is attempted using a physically based approach. Different parameters that enter the model were investigated. The results show that the residual film flow in the macropore is the main driver for abstraction and the physics-based approach contributes only minimally to the abstraction. The event classification and the termination criterion have an influence on the development of the film flow and the water distribution in the soil. The study shows that film flow is applicable in hydrological models and that problems caused by overlapping events can be solved. The physically correct modeling of the abstraction remains a challenge.

Keywords: preferential flow, stokes flow, viscous flow, dual-response model, RoGeR model

Zusammenfassung

Das präferentielle Fließen ist ein nicht zu vernachlässigender Prozess in Bezug auf die Wasserverteilung und den Transport gelöster Stoffe im Boden. In den bestehenden hydrologischen Modellen wird oft versucht, den präferenziellen Fluss als kapillaren Fluss in einem dual-porosity Modell zu beschreiben. Der Stokes- oder viscous flow beschreibt das präferenzielle Fließen als gravitationsgetriebener film flow, der ohne viele Parameter modelliert werden kann. In dieser Machbarkeitsstudie wurde der Versuch unternommen, den stokes flow in das hydrologische Modell RoGeR zu integrieren. Die Abstraktion aus dem film flow in die Bodenmatrix wird versucht mit einem physklaisch basierten Ansatz zu beschreiben. Das Modell wurde für unterschiedliche Parameter analysiert. Die Ergebnisse zeigen, dass der restliche film flow in der Makropore der Haupttreiber für die Abstraktion ist und der physikalisch basierte Ansatz nur minimal zur Abstraktion beiträgt. Die Ereignisklassifizierung und das Abbruchkriterium des flim flows beeinflussen die Entwicklung des film flow und die Wasserverteilung im Boden. Die Studie zeigt, dass der film flow in hydrologischen Modellen anwendbar ist und dass Probleme, die durch überlappende Ereignisse entstehen, gelöst werden können. Die physikalisch korrekte Modellierung der Interaktion zwischen Makropore und Bodenmatrix bleibt eine Herausforderung.

1 Introduction

1.1 What are macropores?

Beven and Germann (1982) distinguish between four different groups of macropores. Pores formed by soil fauna, for example ants, earthworms or moles are of tubular shape, can vary between 1 mm and 50 mm in diameter and are mostly located in the upper soil layers. Pores formed by the outer remains of dead roots can act as water conducting tubes and usually represent 35 % of the soil's volume in a forest. These do however not reach far down. The pores network and its dimension are highly dependent on the existing vegetation. Cracks and fissures are also described by Beven and Germann (1982) as a group of macropores. They contrast with the two previously stated types by not being of tubular shape. As a result of low water content in clay soil, cracks can form in the matrix. The chemical weathering as well as freeze and thaw cycles can also form macropores in bedrock. Natural soil pipes form the last group of macropores. In highly permeable soil with poor structural integrity, high flow velocities can have an erosive effect and form soil pipes below ground.

Bormann and Klaassen (2008) divide macropores in primary macropores caused by soil texture and secondary macropores caused by soil structure. They stress, that soil structure can vary with season and weather. Shrinkage and expansion of clay soils and organic matter can for example be caused by variations in moisture content. Heavy rain can cause collapsing of worm tunnels. Different land use also has an impact on macropores. Heavy equipment can reduce pore volume. Ploughing for example can alternate existing vertical soil structure and interrupt vertical macropore network continuity.

Beven and Germann (1982) mention a dynamic balance between constructive and destructive processes. Macropore networks are constantly being developed by fauna and flora but can also suddenly be destroyed by precipitation events or use of

heavy equipment. In forest soil, predominant flow paths can be stable for decades (Hagedorn and Bundt 2002). Beven and Germann (1982) define macropores as voids that are hydrologically effective in terms of channeling flow through soil. Continuity and connectivity of those voids is critical for channeling water. Size alone does not control macropore flow.

1.2 Importance of macropore flow

The attribute that describes macropores best is channeling of water. Channeling has a significant impact on the flow velocities of water. Water can arrive at greater depths much faster by passing through pores in the soil matrix. This not only influences groundwater recharge but also solute transport. Macropores are particularly relevant regarding the transport of pesticides and other sorbing pollutants (Beven and Germann 2013). Flury (1996) describes how preferential flow paths short-circuit the distance between the ground surface and groundwater. Even strongly absorbing chemicals can quickly reach greater depths. In comparison with matrix drainage the soil water interface is reduced in macropores. Preferential flow affects phosphorus leaching. The sorption capacity of the soil is bypassed and leads to phosphorus loss in the soil (Djodjic et al. 2004). Jarvis (2007) concludes, that macropores will increase the leaching of comparably non-leachable substances, such as strong sorbing pesticides or phosphorus. Preferential flow paths are described as biological hot spots in soils by Bundt et al. (2001). The microbial biomass is higher in macropores due to nutrient and substrate supply. Microbiological activity in macropores can lead to reduced water absorption, as a film can form on the wall of the macropores (Jarvis 2007).

1.3 Preferential flow

Different types of preferential flow are classified according to the mechanisms involved. The two main types are macropore flow and fingering flow. (Germann 2014; Kung 1990) Macropore flow can also be found in the literature classified as short circuit flow (Kung 1990) or non-capillary flow (Coppola et al. 2009). Contrary to macropore flow, fingering can also occur in homogenous matrices (Germann 2014).

Fingering flow is due to an instable wetting front. This can occur when a layer with low permeability meets a layer with high permeability (Coppola et al. 2009, Kung 1990). Jarvis (2007) defines macropore flow as a non-equilibrium process where water close to atmospheric pressure rapidly by-passes a drier soil matrix.

1.4 Modelling preferential flow

Darcy (1856) developed the first equation that quantifies flow in a porous medium. Darcy's model is based on a two phased system, solid and liquid. As such the law only holds under saturated conditions. The hydraulic properties of the permeable medium are described by hydraulic conductivity. This parameter is dependent on the permeable medium and describes the ease with which water is conducted through porous material.

In respect to unsaturated conditions, Richards (1931) introduced his equation for unsaturated vertical flow. The theory is based on capillary forces. The Richards equation as such is only applicable to stable, uniform flow conditions. As a consequence of preferential flow, there is no uniform wetting front. Water can however reach greater depths much faster than the Richards equation would suggest (Šimůnek et al. 2003). Water is flowing macropores ahead of the wetting front in the soil matrix (Jarvis 2007).

Over the last three decades dual-porosity, dual-permeability, multi-porosity and multi-permeability models have been developed to cope with preferential flow. The approach of these models is that different interacting regions are assumed. One region includes macropores and other preferential flow paths and the other region refers to the soil matrix. In the dual porosity model, it is assumed that the water in the soil matrix is stagnant, whereas in the dual permeability model the water in the soil matrix can also flow (Šimůnek et al. 2003).

A popular dual-permeability model is the dual-porosity model from Gerke and van Genuchten (1993) with two separate regions. Both the fracture and the matrix region are treated as homogenous media with separate hydraulic and solute transport properties. The governing equation to describe the flow in both the fracture region and the matrix region is a Darcy-type equation.

Another equation that is used in combination with a dual-porosity model is the Green and Ampt Equation (Heber Green and Ampt 1911). Same as the Richards Equation it is also based on Darcy's law. However, the Green and Ampt equation can be solved analytically. This equation was implemented as a dual-porosity model in the IN3M model by Weiler (2005)).

In contrast to approaches based on Darcy's law, Beven and Germann (2013) advocate for implementation of the kinematic wave equation. Germann (2014) describes the flow in macropores as viscous. A process, that is based on gravity. He applies the kinematic wave theory at a scale much larger than the single macropore.

Beven and Germann (1982) often criticize the application of a Darcy based approach to model preferential flow. In their review they claim that the Richards equation, although widely used, is not adequate to represent the flow processes in a heterogenous unsaturated soil matrix. As such, the dual-porosity and dual-permeability models mentioned before are not appropriate to explain preferential flow. They further claim that most of the soil physics, in respect to infiltration, is based on false experiments conducted by Richards (Beven and Germann 2013).

The Darcy-Richards approach adheres to sequential flow. Under these conditions, bigger pores must empty before smaller pores can, and smaller pores must fill before bigger ones do. In non-equilibrium flow conditions sequential flow is physically not possible as the progression of the wetting front in the matrix cannot keep up with the faster processes in the macropores. Viscous flow on the other hand is only gravitational based and can be non-sequential (Germann and Karlen 2016).

In the foreword of Peter Germann's Book *Preferential Flow - Stokes Approach to Infiltration and Drainage*, Keith Beven summarizes why the Darcy Richards approach is still commonly used for modelling soil infiltration (Germann 2014), even though many papers provide proof that the Richards equation is not applicable in most field soils (Weiler 2017). Beven gives possible explanations for why the Darcy-Richards approach has still not been rejected. One reason is because today's conceptual models, with some calibration and without consideration of flow paths, manage to predict discharges. Another is that with a wide range of new, readily available and easy to use software packages that are based on Darcy-Richard's equation, as well as steadily increasing computing power needed for calculations, the Darcy-Richards approach has become more accessible. In the next section, the

film flow model by Peter Germann will be discussed in more detail.

1.5 Film flow model by Peter Germann

Beven and Germann (1981) characterised macropore flow as viscous flow. Germann, Peter (1985) applied the kinematic wave theory to the infiltration and redistribution of a single square pulse of water in the macroporous system of a porous medium. This approach is only applicable for saturated soils, since no abstraction from the macropore into the soil matrix is considered. The coefficients for the kinematic wave approach were experimentally determined. Germann and Beven (1985) included a sink function into the kinematic wave theory approach. The sink term accounts for the sorption from the macropore flow by the surrounding soil matrix. This approach to quantify the amount of abstracted water from the macropore flow was declared as unfit by Germann (2014) and Hincapié and Germann (2009b). Germann and Di Pietro (1999) state, that the preferential flow is governed by the dissipation of momentum due to viscosity. The movement in finer pores is in contrast dominated by diffusion of capillary momentum. The approach of Germann and Di Pietro (1999) is based on Newton's law of shear stress. During preferential flow or propagation of the water content wave, Newton's shear stress force acts against gravity. The term mobile volumetric soil moisture is defined and later renamed to mobile water content. Germann (2014) goes into detail about the derivation of this approach based on Newton's shear force. As the approach from Germann and Di Pietro (1999) is a simplification of the Navier-Stokes equation, the flow is also called Stokes-flow.

The water content wave (WCW) approach was introduced by Germann et al. (2007) and evaluated by Hincapié and Germann (2009a). Germann (2014) formulated conditions for the application of the WCW.

1. All flow arriving at the surface continues as WCW, no ponding occurs.
2. Conditions of flow prevail along the flow paths during the existence of the WCW. (This condition does not mandatorily require a homogeneous pore system).
3. The WCW neither loses nor gains water.
4. There is no viscous flow in the permeable medium prior to the arrival of the pulse.

Condition 3 is later relaxed as one must account for abstraction from the water content wave into the soil matrix.

The WCW approach is further developed with the application of the kinematic wave-theory. The WCW approach can only predict the propagation of a single rectangular input pulse. If a variable input pulse is infiltrated, the simple approach of the WCW is no longer applicable. This case is described as a cascading input. Lighthill and Whitham (1955) initially developed the kinematic wave theory for flood movements along rivers and traffic flow.

Although the original model had a sink term that was applied on the water content wave (Germann and Beven 1985), the film flow model developed by Germann and Beven is mostly described without an abstraction term (Germann and Prasuhn 2018, Germann 2014). When describing the theory for a single input pulse and the propagation of that single pulse, one of the four prerequisites for the viscous flow is the absence of abstraction from the water content wave. The total volume of water applied to the soil surface remains preserved within the WCW as there are neither gains nor losses to and from the WCW Germann and Karlen (2016). If one were to apply the film flow model without abstraction, the film flow would carry all the water with it and eventually, all water would drain into the groundwater. However, when looking at the volumetric water contents in soil profiles with time domain reflectometry equipment, the volumetric water content after the WCW has passed (θ_{out}) is higher than it was at the beginning (θ_{in}). Hincapié and Germann (2009b) compared the theoretical WCW of the film flow to an observed WCW measured with time-domain reflectometry (TDR) equipment. The rate of the measured water content increase from θ_{in} to θ_{max} is defined as the temporary abstraction attributed to water sorption. The difference between θ_{in} and θ_{out} is defined as the definitive water abstraction from the WCW, which represents a loss from the WCW. Hincapié and Germann (2009b) as well as Demand and Weiler (2021) suggested a linear regression approach to assess the abstraction from the water content wave. However, with the goal of implementing the stokes flow approach in the hydrological model Roger (Steinbrich et al. (2016)) a more physical approach is necessary.

1.6 The hydrological model RoGeR

The hydrological model RoGeR is a soil hydrological model that was developed at the University of Freiburg. RoGeR stands for Runoff Generation Research. The model is physically based, and calibration is not required. Processes are simulated with a high temporal and spatial resolution. The model was first developed to quantify runoff processes. The model is constantly evolving and can be found under different forms. The processes of water balance and runoff concentration can be found in the further developments. The model exists among others as a raster-based runoff and soil water model (RoGer_WB). The time stepping of the model is process dependent. During a precipitation event, it is calculated in 10-minute or hourly time intervals. In periods without precipitation, the redistribution in the soil and the evaporation are calculated daily. This change in temporal resolution is made to ensure fast computation, even when modeling longer periods.

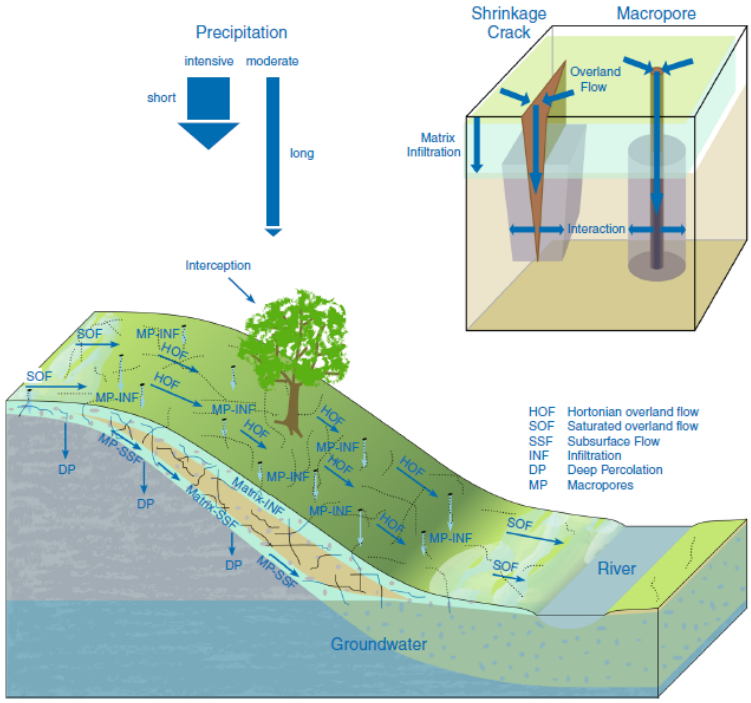

Figure 1.1: Schematic representation of the processes implemented in RoGeR. (Steinbrich et al. 2016)

In the RoGeR model, a whole series of processes are considered. The runoff generation process is split in several runoff components. Implemented are Hortonian overland flow (HOF), due to infiltration excess. The saturated overland flow (SOF) resulting from a fully saturated soil. Subsurface flow (SSF) is again split in a

slow component through the soil matrix and a fast component through the lateral preferential flow paths. Deep percolation into groundwater is also considered in the model. Infiltration is modelled with the Green-Ampt-Method. RoGeR also accounts for infiltration through macropores and shrinkage cracks. Depending on the macropore density of the soil, a part of the Hortonian flow, if present, will pass into the preferential flow paths. From the two preferential flow paths, macropores and shrinkage cracks, infiltration into the soil matrix is calculated via the Green-Ampt method.

In the RoGeR_WB version the evaporation is included in the water balance. Evaporation is calculated based on the interception storage of the trees, water surfaces and the shrub and grass layer. Evaporation and sublimation from the snow cover are also considered.

The soil storage is divided into two layers. The root zone representing the upper layer, and the subsoil representing the lower layer. The soil is defined by three main parameters. Usable field capacity, the air capacity or drainable porosity and the permanent wilting point. Evaporation takes place only in the upper soil layer. The water percolating from the subsoil is considered as groundwater recharge and called deep percolation.

Runoff concentration, snow accumulation and storage, as well as urban processes are also considered in the Roger model. This will however not be detailed any further in this thesis, as it is not considered in the 1D version.

The Roger model Roger_WB also exists as a 1D version (RoGeR_WB_1D). This is particularly suitable for quickly modeling the soil water balance. Lateral processes are not considered in this version.

1.7 Research gap

Demand and Weiler (2021) have taken up the years of research by Peter Germann and Keith Beven. They confirmed the physical relationship between the wetting front relationship and rain pulse input.

A problem that is mentioned repeatedly is the water abstraction from the film

flow of the macropore into the surrounding soil matrix. As specified in condition 3 for the WCW, in most cases it is assumed that no abstraction from the WCW takes place. Germann and Beven (1985) tried to describe the abstraction from the WCW with a sink term. As stated in Germann (2014) this approach failed entirely when applied to the water-content version of the viscous flow. Hincapié and Germann (2009b) applied multiple linear regression to explain the deviations between the observed and theoretical WCW, hence the abstraction. DiPietro et al. (2003) added a diffusive part to the kinematic wave theory to account for water abstraction. The Demand and Weiler (2021) approach, based on Hincapié and Germann (2009b) uses a multiple linear regression model to predict the abstraction. The goal however is to find a more physics-based approach to describe the abstraction from the water content wave. Furthermore, the goal is also to use as few parameters as possible.

The film flow model has yet to be implemented in a hydrological model. Therefore, the goal of this research is to incorporate the film flow into the RoGeR model and identify possible hurdles that arise during this implementation.

1.8 Procedure

The implementation of the stokes flow into the hydrological model RoGeR can be divided into two phases. In the first phase, the functions to describe the different processes were developed. The main difficulty is to account for the abstraction from the macropore flow. Subsequently, the functions were tested on single events and the modeled data was compared with the observed data. In a second phase, the single event approach developed in first phase was introduced into the RoGer model and modeled data was compared with the observed data from the lysimeter.

2 Data

The data used for the verification of the approach was obtained from the large-scale lysimeter facility in Zurich-Reckenholz (Prasuhn et al. 2009). The soil is sandy-loamy parabasic soil over ground moraine. The monolith has a height of 150 cm and a surface area of 1 m^2. The lower 15 cm of the monolith was replaced with a gravel filter. The time series ranges from January 1, 2016, to December 31, 2017. The resolution of the data is given in 10-minute intervals. Soil water content was determined by Frequency Domain Refelectometry (FDR) probe at the depths of 10, 30, 60 and 90 cm. Additional parameters included in the data set are precipitation (in mm/10min), air temperature (in °C), potential evapotranspiration (in mm/10min), percolation (in mm/10min) and the lysimeter weight (in kg). Ground parameters of the monolith are provided in an additional table. Values of the soil analysis of the Lysimeter plant can be taken from an attached table. In this table, soil parameters such as grain size or saturated hydraulic conductivity can also be found.

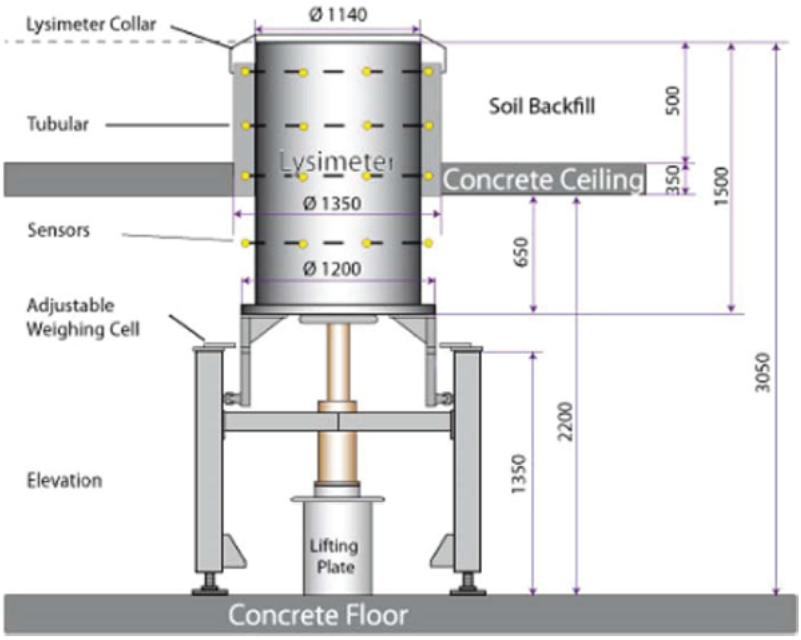

Figure 2.1: Design of the free draining weighable lysimeter. (Germann and Prasuhn 2018)

In addition to the raw lysimeter data, a time series with corrected precipitation data was used for further analysis. This dataset was determined by accounting for the weight increase and percolation of the lysimeter. The use of this corrected time series is important because, in addition to the natural precipitation input, experimental irrigation was also carried out at certain periods.

3 Methodology

3.1 Phase I: Developing the functions for single events

The film flow as well as the abstraction will be tested in a first phase on single events. For the modeling of the film flow, I primarily relied on Germann and Prasuhn 2018. The rectangular input pulse method is used, which can be described with a WCW. The progression of the wetting front is described with the kinematic wave theory for the viscous flow.

The technique used for further calculations is strongly based on Demand and Weiler (2021). They developed the method to determine the input pulse of a rainfall event based on cumulative rainfall.

3.1.1 Manual calculation of film flow velocities

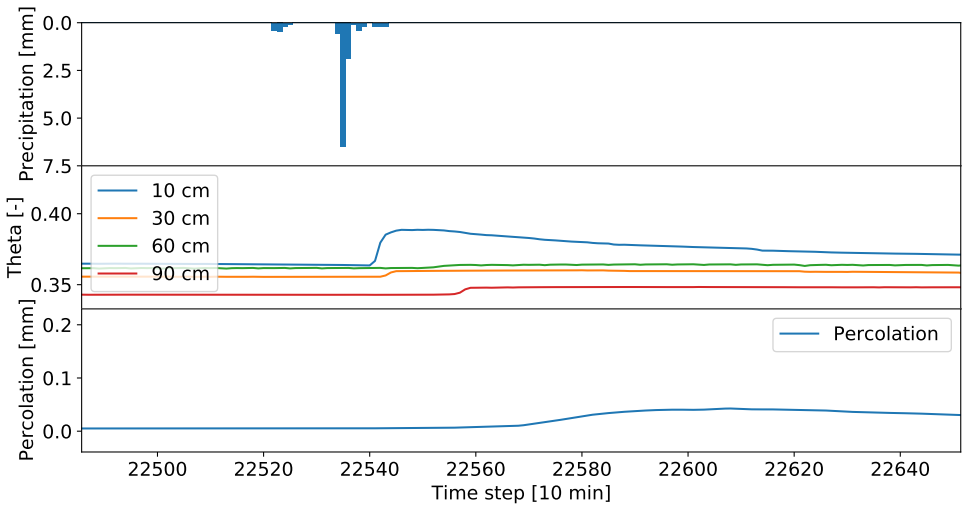

Figure 3.1: Sample of data used in the study: precipitation data; volumetric water contents recorded with frequency domain reflectometry; drainage collected by the lysimeter.

In a first step, the film flow velocity must be calculated manually for various events. These velocities are used in the next section to parameterize the film flow. I looked at time series of volumetric water content at different depths for the given lysimeter data (Chapter 2). I manually selected events, where an increase in the volumetric water content was clearly discernible at all depths. The selected events should, if possible, not have been influenced by previous or following events. To define the precise wetting front arrival time of the water content wave, I used an approach described in Germann (2017). For every selected event and every given depth, I visually determined the volumetric water content at the beginning, in the following described as θ_{lo} [-] as well as the maximum volumetric water content, in the following referred to as θ_{up} [-]. Having defined θ_{lo} and θ_{up}, the equation 3.1 gives the water content increase $\Delta\theta$.

$$\Delta\theta = \theta_{up} - \theta_{lo} \tag{3.1}$$

A linear regression model applied to the volumetric water content values between θ_{lo} and θ_{up} gives the arrival time of the wetting front T_W (s), when the volumetric water content is equivalent to $\theta_{lo}+ \Delta\theta/2$. The arrival time was calculated for every selected event and every given depth.

$$T_W = T_B + \frac{1}{u}\left(\theta_{lo} + \frac{\Delta\theta}{2} - \theta_0\right) \tag{3.2}$$

As described by Germann and Prasuhn (2018) the slope of the linear regression of the instrument depth and the previously calculated arrival times of the wetting front represents the average wetting front velocity for an event.

3.1.2 Determination of the input pulse

The film flow model is based on uniform rain input for each event, described as an input pulse. To define the pulse intensity and the duration of that pulse a method developed by Demand and Weiler (2021) was used. In order to determine the pulse, the data of the cumulative precipitation of the considered event was used. A linear regression was fitted to the data between the 0.25 percentile and the 0.75 percentile. The beginning of the pulse was determined by the x-intercept of the linear regression.

The end of the pulse was determined at the point where the linear regression reaches the value of the accumulated precipitation. The intensity of the input pulse is given by the slope of the linear regression.

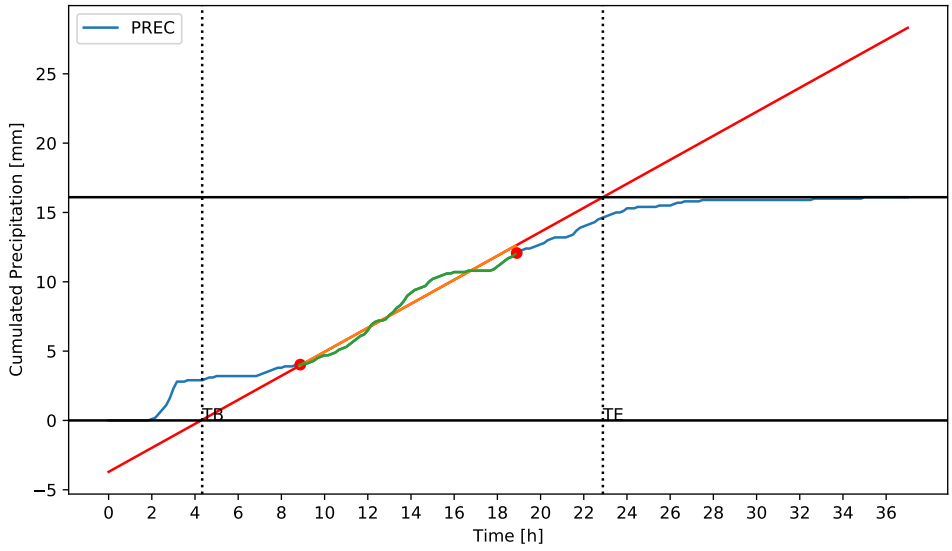

Figure 3.2: Transformation of a rainfall event to define qs, TB and TE of the input pulse.

3.1.3 Calculation of the film flow

To describe the progress of the wetting front in the soil, the velocity of the film flow must be determined. Demand and Weiler (2021) describe how to derive the velocity of the film flow from the input pulse. The integration of the differential flux from the soil-water interface to the air-water interface amounts to the volume flux density q [LT^{-1}] of the film flow:

$$q(F, L) = \frac{g}{3\eta} L F^3 \tag{3.3}$$

where g is the acceleration of gravity [LT^{-2}] and η is the kinematic viscosity of water [$\mathrm{L}^2\mathrm{T}^{-1}$].

The mobile water content w [-] is given by:

$$w(F, L) = F \cdot L \tag{3.4}$$

where F [L] is the film thickness and L [L^2L^{-3}] the length of the contact of the soil water interface. In general, the wetting front velocity v [LT^{-1}] can be determined form the volume flux of the water film $q(F, L)$ and the mobile water content wave $w(F, L)$:

$$v(F) = \frac{q(F, L)}{w(F, L)} = F^2 \frac{g}{3\eta} \tag{3.5}$$

Combining Equation 3.3 and Equation 3.5 by eliminating F gives the wetting front velocity v based on the volume flux q and length L of the contact area of the soil water interface:

$$v(q, L) = q^{2/3} \left(\frac{g}{3\eta}\right)^{1/3} L^{-2/3} \tag{3.6}$$

The macropore restriction for viscous flow [dL/dq = 0] implies, that L is stable (Germann 2014). From this follows the Equation 3.7, where qs is the only variable in the Equation:

$$v(q_s) = q_s^{2/3} \left(\frac{g}{3\eta}\right)^{1/3} L^{-2/3} \tag{3.7}$$

Demand and Weiler (2021) defined a velocity-modulation coefficient a for the Equation 3.8:

$$a = \left(\frac{g}{3\eta}\right)^{1/3} L^{-2/3} \tag{3.8}$$

The velocity-modulation coefficient can be associated to landscape properties, such as the geology or the landcover. As such the Equation 3.8 can be rewritten:

$$v(q_s) = aq_s^b, b = \frac{2}{3} \tag{3.9}$$

The parameter b was experimentally determined to be 2/3 in case of macropore flow by Hincapié and Germann (2009a). Plotting v against qs in a log-log diagram results in a linear regression describing the parameters of Equation 3.9. Applying the logarithm to Equation 3.9 results in Equation 3.10, where the slope of the linear regression is determined by the parameter b and the intercept is given by the term log(a) of Equation 3.10.

$$log(v) = log(a) + log(q) \cdot b \tag{3.10}$$

In order to determine the parameter a for the lysimeter soil used, the relationship of $v \approx q_s^{2/3}$ was used as described above. The input for v was given by the average film flow velocities determined in section 3.1.1 and the input pulse calculated under section 3.1.2 was used as q_s in the linear regression. Fitting a linear model to the logarithmic data gives log(a) as the intercept of that model. I applied the function curve_fit form the scipy.optimice package with parameter b set to 2/3.

Knowing the input pulse, drawn from the precipitation of the event, and knowing the landscape parameter a derived from Equation 3.10, the film flow velocity of a given event can be calculated. The parameter a describes to a certain degree the soil structure of our lysimeter, since it includes the parameter L (Eq.3.8).

3.1.4 Film flow modeling in macropores

Knowing the film flow velocity, allows to describe the progression of the film flow in macropores. The used approach is strongly based on the method described by Germann and Prasuhn (2018). The basis for the modeling of the film flow is the input pulse, which is derived from the cumulated precipitation obtained using the method described in section 3.1.2. A free-surface flow a long a vertical plane is assumed as geometry. The input pulse of an event is defined by its start point T_B [T], its end point T_E [T] and its intensity q_s [LT^{-1}]. The total volume of the WCW V_{WCW} [L] can be described with the following three parameters:

$$V_{WCW} = q_s \left(T_E - T_B\right) \tag{3.11}$$

The wetting front velocity is given by the Equation 3.9 derived in section 3.1.3. After the cessation of the input pulse at T_E, the drainage front appears. The celerity c [LT^{-1}] is the wave velocity of the drainage front and is given by the Equation 3.12:

$$c = \frac{dq}{dw} = 3v \tag{3.12}$$

Since the drainage front is three times faster than the wetting front (Eq. 3.12), both fronts intersect at a given time T_I [T] (Eq. 3.13) an depth Z_I [L](Eq. 3.14).

$$T_I = \frac{1}{2}\left(3T_E - T_B\right) \tag{3.13}$$

and

$$Z_I = \frac{c}{2}\left(T_E - T_B\right) \tag{3.14}$$

Since the single event model is to be incorporated into the hydrological model RoGeR at a later stage, two soil layers are already modeled in the single event approach as well.

Within $0 \leq z \leq Z_I$ the positions of the wetting z_W [L] front and drainage z_D [L] front are given by the Equations 3.15 and 3.16 as a function of time:

$$z_W(t) = v(t - T_B) \tag{3.15}$$

and

$$z_D(t) = c(t - TE) \tag{3.16}$$

The arrival times of the wetting front t_W [T] and drainage front t_D [L] are given as a function of z:

$$t_W(z) = T_B + \frac{z}{v} \tag{3.17}$$

and

$$t_D(z) = T_E + \frac{z}{c} \tag{3.18}$$

After the intersection at T_I the wetting front starts to decelerate as it intercepts

the drainage front at Z_I. The drainage front disappears and only the wetting front persists. The position and the arrival time of the wetting front is given by the Equation 3.19 and 3.20.

$$z_W(t) = c(t - T_E)^{1/3} \left(\frac{T_E - T_B}{2} \right)^{2/3} \tag{3.19}$$

and

$$t_W(z) = T_E + 4 \left(\frac{z}{3} \right)^3 (T_E - T_B)^{-2} \tag{3.20}$$

The volume fluxes of the film flow need to be considered for different periods depending on the position of the wetting front. Because the RoGeR model only calculates in two different layers, the water that is in the film flow, is also calculated on the entire layer. This is important, because the water balance later used in the RoGeR model also refers to the entire layer. For this reason, I calculate what flows into and out of the layer, for each time step. The inflow into the rootzone layer is given by the input pulse. The following periods need to be considered:

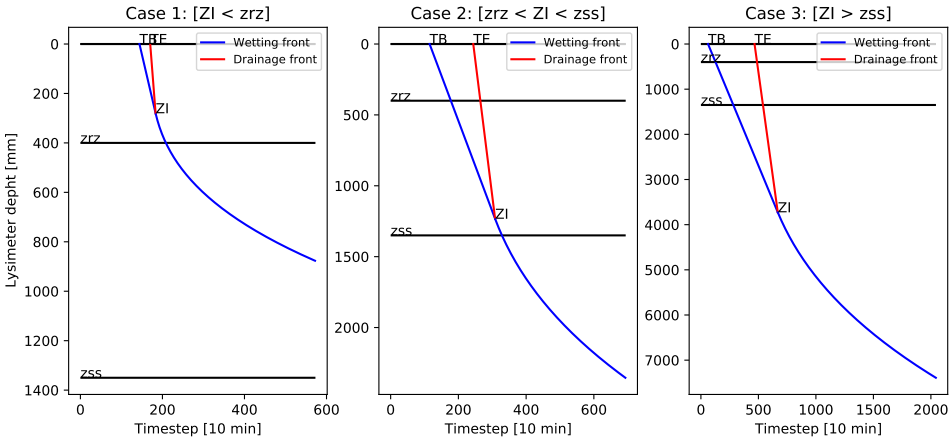

Figure 3.3: When modeling the film flow, three different cases need to be considered. Case 1: the intersection is in the root zone; Case 2: the intersection is in the subsoil; Case 3: the intersection is below the soil layer.

$t \leq T_B$:

$$q(z,t) = 0 \tag{3.21}$$

$T_B \leq t \leq T_E$:

$$q(z,t) = q_s \tag{3.22}$$

$t_D(z) \leq t \leq T_I$:

$$q(z,t) = qs \left[\frac{t_D(z) - T_E}{t - T_E}\right]^{3/2} \tag{3.23}$$

$t \leq T_I$:

$$q(z,t) = \frac{V_{WCW}}{2} \left[t_W(z) - T_E\right]^{1/2} (t - T_E)^{-3/2} \tag{3.24}$$

3.1.5 Abstraction from the film flow

The interaction between the macropore and the soil matrix is described by the abstraction. The abstraction represents the water portion of the film flow, which is abstracted into the soil matrix when flowing through the macropore. This part is often neglected by the film flow model of Peter Germann. However, it can be assumed that part of the water is retained in the soil matrix.

With the intention of incorporating the film flow model into the process-based model, the goal is to describe the abstraction with a physics-based approach.

The abstraction I [LT^{-1}] into the soil matrix is calculated with Equation 3.25:

$$I = \theta_{d_{rel}} \cdot \Psi \cdot K_s \cdot f \cdot dz_{wf} \cdot dt \tag{3.25}$$

where $\theta_{d_{rel}}$ [-]is the relative soil moisture deficit, Ψ [L] is the wetting front suction, K_s [LT^{-1}] is the saturated hydraulic conductivity, f is an optional fudge parameter scaled between 0 and 1 and dz_{wf} is the change in wetting front depth [L] .

The wetting front suction Ψ [L] is calculated in the RoGeR model with a Brooks and Corey approach (Brooks and Corey (1964)). The soil moisture deficit $\theta_{d_{rel}}$ [-] is calculated relative to the permanent welting point and the saturation of the soil:

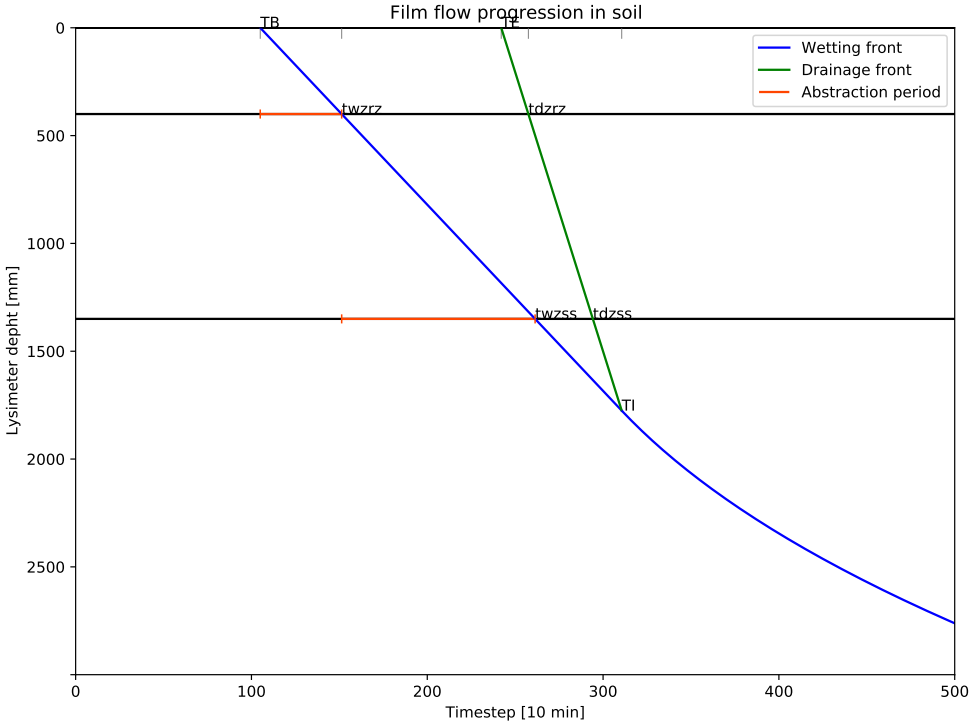

Figure 3.4: Abstraction period for single abstraction. Abstraction ends when the wetting front reaches the bottom of the layer.

$$\theta_{d_{rel}} = \frac{\theta_{sat} - \theta_{init}}{\theta_{sat} - \theta_{pwp}} \tag{3.26}$$

The abstraction is calculated individually for each soil layer. The model assumption is that an abstraction into the soil matrix only occurs during the initial wetting of the macropore wall. This approach is later referred to as single abstraction. The abstraction into the soil matrix depends on the water content of the soil. During an event the abstraction is calculated based on the initial volumetric water content (θ_{init}) of the soil layer.

The assumption of single abstraction will be relaxed later. For the single event approach, a continuous abstraction is also tested. The continuous abstraction is later referred to as a long abstraction. The abstraction is calculated over the entire length of the wetted wall and is calculated until the end of the film flow, or until there is no more water in the layer.

The abstraction calculated on this physics-based approach is later also referred to as direct abstraction. Later in the hydrologic model, the residual water at the end of the film flow event is also abstracted into the soil matrix. This approach is however physically contradictory and will be discussed later.

3.1.6 Defining the end criterion

Defining an end criterion for the film flow process is necessary, because the kinematic wave approach is an asymptotic process. At any given depth, without considering the abstraction, the cumulated flow would converge to the total volume of the WCW V_{WCW}. Being an asymptotic process, this drags on to infinity, until the entire water fraction V_{WCW} flows past. The end criterion is therefore necessary to prevent the film flow from being calculated infinitely.

The end criterion is also used to stop macropore flow in the RoGeR model and to start the redistribution in the soil via capillary processes. The end criterion can be defined in multiple ways. One option would be to assume that after the intersection of the wetting front and the drainage front the film flow is negligible. Given this assumption, the termination of the film flow would be at time TI.

Alternatively, the volume flux density q_s can be used to define the end criterion. The end criterion is set when the volume flux density from the soil layer reaches a defined percentage of the input volume flux density q_s. The percentage for the end criterium is given by the parameter ptc (percentage of the termination criterion) and can be adjusted in the parameter file. The end of the film flow is determined when the volume flux density reaches q_{end} (Eq. 3.27).

$$q_{end} = ptc * q_s \tag{3.27}$$

Solving Equation 3.28 for t gives the end time of the film flow event.

$$q_{end} = q_s \left[\frac{T_I - T_E}{t - T_E} \right]^{3/2} \tag{3.28}$$

3.2 Phase II: Implementation of the Stokes flow in the existing RoGeR Model

The film flow in the RoGeR model is calculated in the same way as in the approach for the individual events. Since the RoGeR model is a water balance model, other processes are considered in addition to infiltration into the soil. RoGeR considers interception and evaporation. As such, the precipitation is not completely available for infiltration into the soil.

Another characteristic of film flow that can lead to problems when modeling multiple events is the overlapping of film flow events. Germann (2014) mentions the propagation of an increasing or decreasing jump. This is the case, when the input pulse changes its intensity. In both cases, one would have to apply a different set of functions to model the propagation of the wetting fronts. In this research, I am not considering jump cases, as I am only modeling the propagation of a single, constant pulse. Nevertheless, as mentioned above, when modeling several events, an overlapping of wetting fronts can occur(Fig. 3.5). One would have to calculate the progress of the wetting fronts and fluxes for two or possibly more events at the same time. The simultaneous calculation of different events would require a much more complex approach.

The advantage of the film flow approach is, that the entire sequence of the film flow can be calculated with the input parameters. The parameters are event specific and are constant over the duration of the event. Roger classifies in advance the input data for the precipitation into individual events based on the intensity of the precipitation. During precipitation periods and depending on precipitation intensity, Roger calculates in 10 minute or hourly intervals. In precipitation-free periods, Roger performs calculations daily. The film flow process continues even after the end of the precipitation and must be calculated with the highest possible temporal resolution. The extent of an event is recalculated based on the end criterion and the temporal resolution is set to 10 minutes for all events, regardless of intensity. A number is assigned to each event.

After the preprocessing of the input data the actual modeling takes place. The Roger model iterates over the time steps defined in the pre-processing until an event starts. At the beginning of the event, the event-based parameters are derived. Based

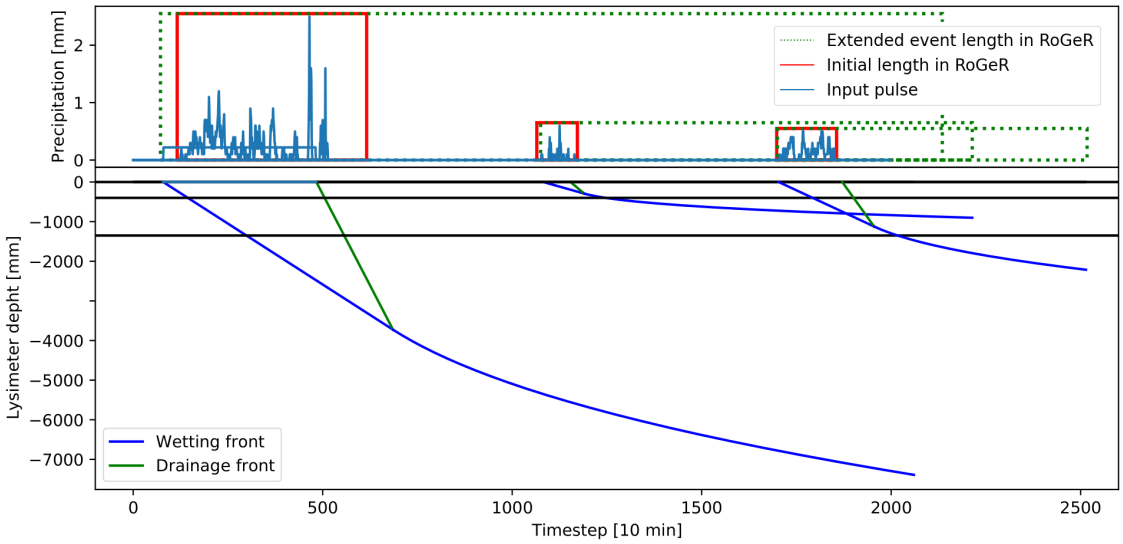

Figure 3.5: Synthetic example of three film flow events where the wetting front of event 1 overlaps events 2 and 3 and the wetting front of event 2 overlaps event 3.

on these parameters we can calculate the complete potential film flow series for a given event and store it in a dictionary. To avoid the problem of overlapping film flow events, the potential water content of the individual events is summed up for each time step and stored as a summed film flow. Later, when iterating over the time steps, the potential water content is no longer calculated directly. The value is fetched from the summed film flow. Figure A.1 shows a simplified schema of the model. The package for the hydrological model RoGeR including the film flow is available in a GitHub repository (Schwemmle 2021).

4 Results

4.1 Manual calculation of film flow velocities

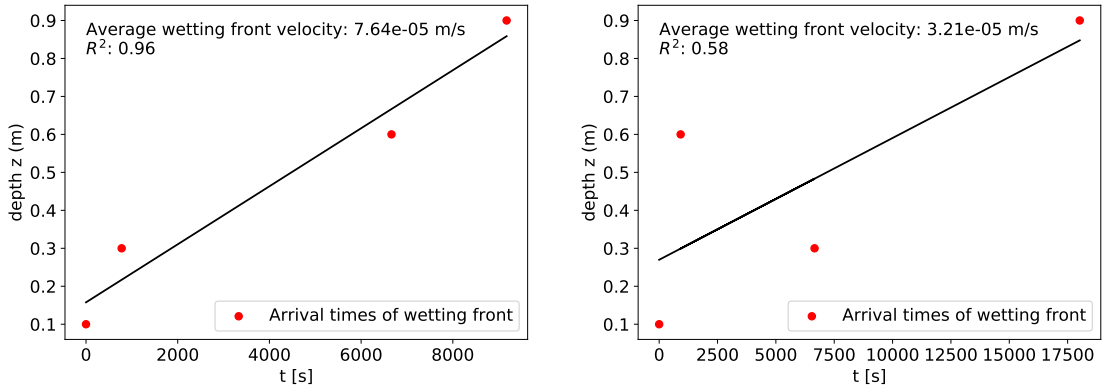

(a) **(b)**

Figure 4.1: Average film flow velocity defined by the arrival time of the wetting front.

The film flow velocities for the selected events reach from a minimum of $8.7 \cdot 10^{-6} ms^{-1}$ to a maximum of $7.64 \cdot 10^{-5} ms^{-1}$. For the event 22520 the arrival time of the wetting front at different depths is consecutive. In figure 4.1b we can see that the wetting front first arrives at a depth of 0.6 m and later of 0.3 m. The same behavior is observed in event 59519. The low coefficient of determination for the event 61068 and 59519 are reflected by these values.

Table 4.1: Film flow velocities and volume flux densities

Event ID	Velocity [m/s]	R2	qs [m/s]
22520	7.64E-05	0.96	1.08E-05
31212	2.05E-05	0.86	7.86E-07
42651	1.35E-05	0.85	4.65E-07
59519	8.70E-06	0.68	4.17E-07
61068	3.21E-05	0.58	1.66E-06

4.2 Determination of the input pulse

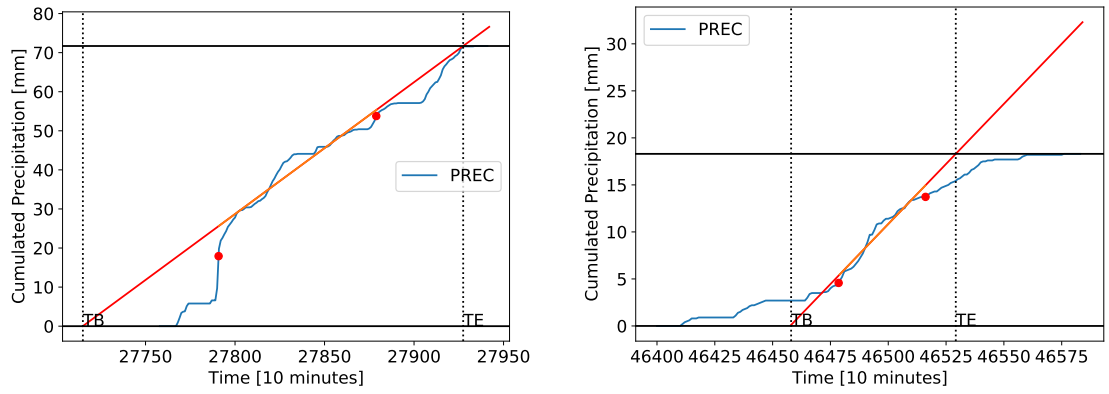

Figure 4.2: Calculation of T_B, T_E and q_s of the input pulse for two example events.

The determination of the start and end point of the input pulse does not coincide with the precipitation event. In figure 4.2a the start point T_B is set too early, the end point T_E is mapped almost correctly. In figure 4.2b the T_B is set too late and T_E too early.

Table 4.2: Difference of the modeled start and end points T_B and T_E, from the observed start and end points T_b and T_e.

ID	tb[10min]	te[10min]	TB[10min]	TE[10min]	TB-tb[10min]	TB-tb[h]	TE-te[10min]	TE-te[h]
19025	19025	19415	18980	19384.35	-45	-7.5	-30.65	-5.10
20606	20606	20753	20604	20772.35	-2	-0.33	19.34	3.22
27769	27769	27935	27715	27927.45	-54	-9	-7.54	-1.25
31213	31213	31280	31202	31257.12	-11	-1.83	-22.88	-3.81
42651	42651	42749	42698	42725.58	47	7.83	-23.41	-3.90
46410	46410	46577	46458	46529.2	48	8	-47.79	-7.96
56960	56960	57228	57064	57201.07	104	17.33	-26.93	-4.48
62291	62291	62492	62307	62418.31	16	2.66	-73.69	-12.28
70968	70968	71032	70978	71020	10	1.66	-12	-2
				Average:	12.55	2.09	-25.06	-4.17

The modeled start and end points of the precipitation events deviate strongly from the observed values (Tab.4.2). On average, the modeled starting point Tb is 2.09 hours behind the actual starting point. The largest deviation is found at event 56960 and amounts to 17.33 hours. A tendency of whether the start point is modeled too early or too late can't be clearly determined. On average, the end point is calculated 4.17 hours too early. The largest deviation is with 12.28 hours at event 62291. Apart from event 20606, the end point is calculated too early in all cases.

The table A.1 lists the observed lengths of the events, maximum length of non-precipitation periods and the deviations of the starting point for different events. There is a correlation between the maximum length of the non-precipitation periods and the deviation of the input pulse start point to the observed start point. The Pearson coefficient of 0.714 expresses a positive linear relationship between the two variables (A.2).

Table 4.3 shows the summed precipitation values of the input pulse for selected events. The values of the input pulse result from the calculated volume flux density and the time span between TB and TE. For comparison the observed precipitation values are also shown in table 4.3. The modeled and observed values differ in their decimal places.

Table 4.3: Comparison of the modeled and observed precipitation data

Event ID	19025	20606	27769	31213	42651	46410	56960	62291	70968
P calc [mm]	90.444	23.164	71.681	26.037	7.700	18.192	51.085	16.057	11.524
P obs [mm]	90.5	23.2	71.7	26.1	7.6	18.3	51.2	16.1	11.6

4.3 Parameterisation of film flow process

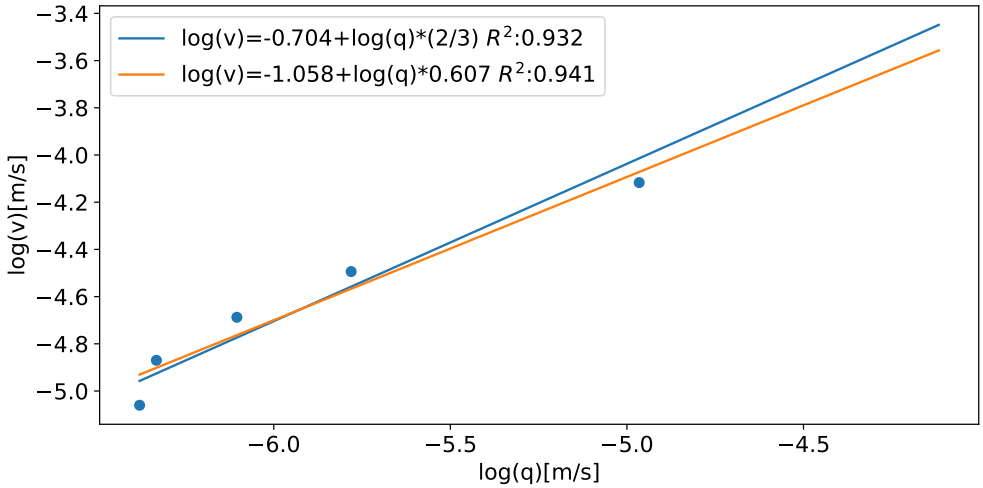

Figure 4.3: Determination of parameter a

The parameter a is decisive for the determination of the film flow velocity (Eq. 3.9). The linear regressions of the loglog relationship between v and qs are shown in the figure 4.3. The orange line corresponds to the linear regression with two free

parameters a and b. The blue line describes the linear regression with only one free parameter a and the constant parameter b set to 2/3. The calculated parameter a is with a value of 0.607 close to the ideal value of 2/3. With 0.932, respectively 0.941, the goodness of fit is very high for both models. The linear regression also describes the distribution of the values quiet precisely.

4.4 Film flow simulations for single events

Figure 4.4 shows the simplest approach to model the film flow. The film flow ends at depth Z_I and at time T_I. The abstraction into the soil is only considered for the initial wetting. The abstraction is small and not visible in the figure 4.4. The residual film flow remains in the root zone and the subsoil. In this case Z_I is above the end of the subsoil and the film flow does not reach the groundwater.

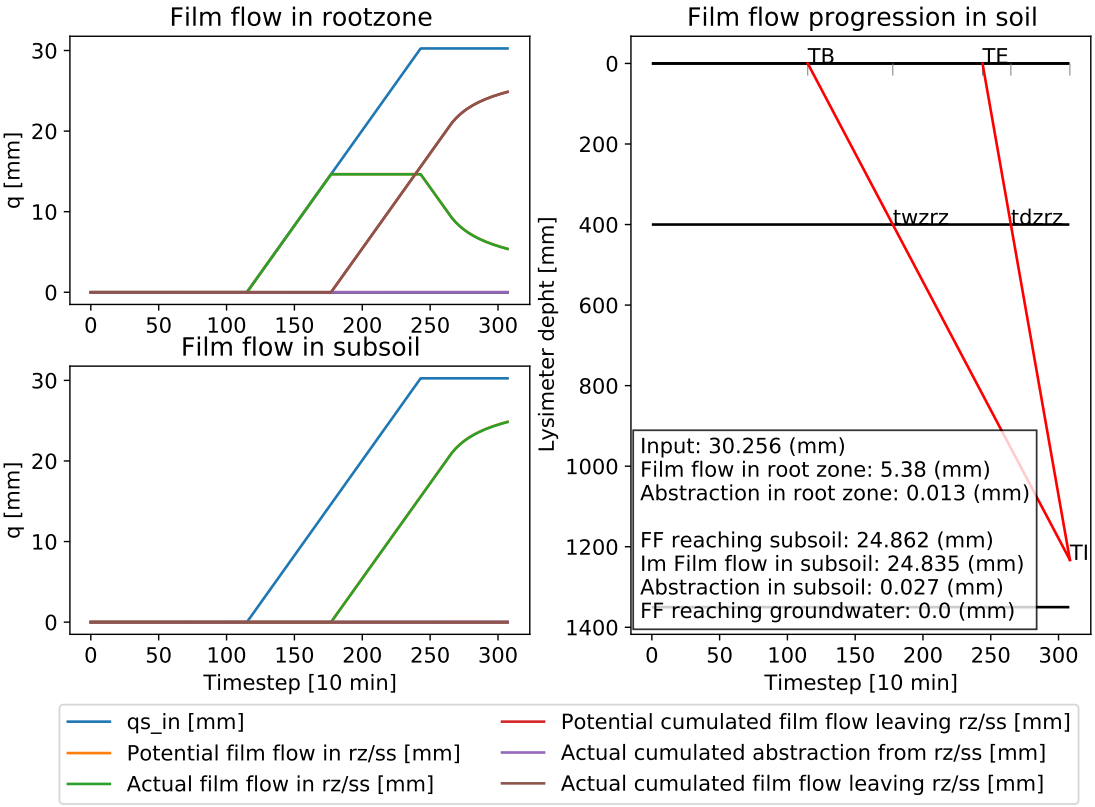

Figure 4.4: Film flow modeling for event 81100 with termination criterion at Z_I and single abstraction.

Figure 4.5 shows the same event as in figure 4.4. The termination criterion is 1%

of q_s and the abstraction is calculated at the initial wetting. The continuation of the film flow after Z_I ensures that water enters the groundwater. A residual portion of the film flow is not directly abstracted and remains in the root zone and in the subsoil after the end of the film flow. The abstraction is so small that the potential film flow is not visually different from the actual film flow in the graphic below. In reality there is a difference. Only 0.06% of the input is abstracted in event 88100.

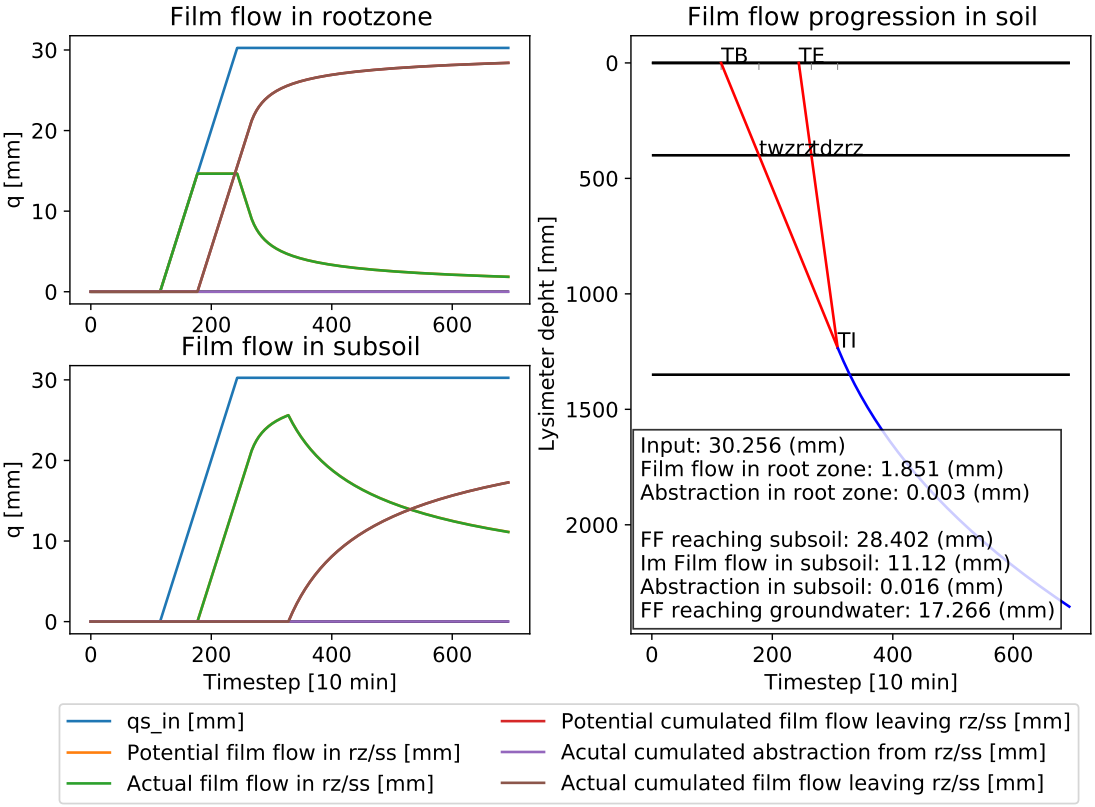

Figure 4.5: Film flow modeling for event 81100 with termination criterion at 1 % and single abstraction.

Figure 4.6 shows event 81100 modeled with a long abstraction period. Here, water is continuously withdrawn from the film flow into the soil as the wetting front progresses. The potential film flow differs visibly from the actual film flow. At the end of the event, the remaining film flow in the root zone and subsoil is less than for the single abstraction model 4.5. The outflow to groundwater remains unchanged for this event.

Figure 4.7 shows the results of different models for events of different intensities and durations. The observed percolation of the lysimeter was used as reference, shown here in red. The outflow of the models shown corresponds only to the film flow

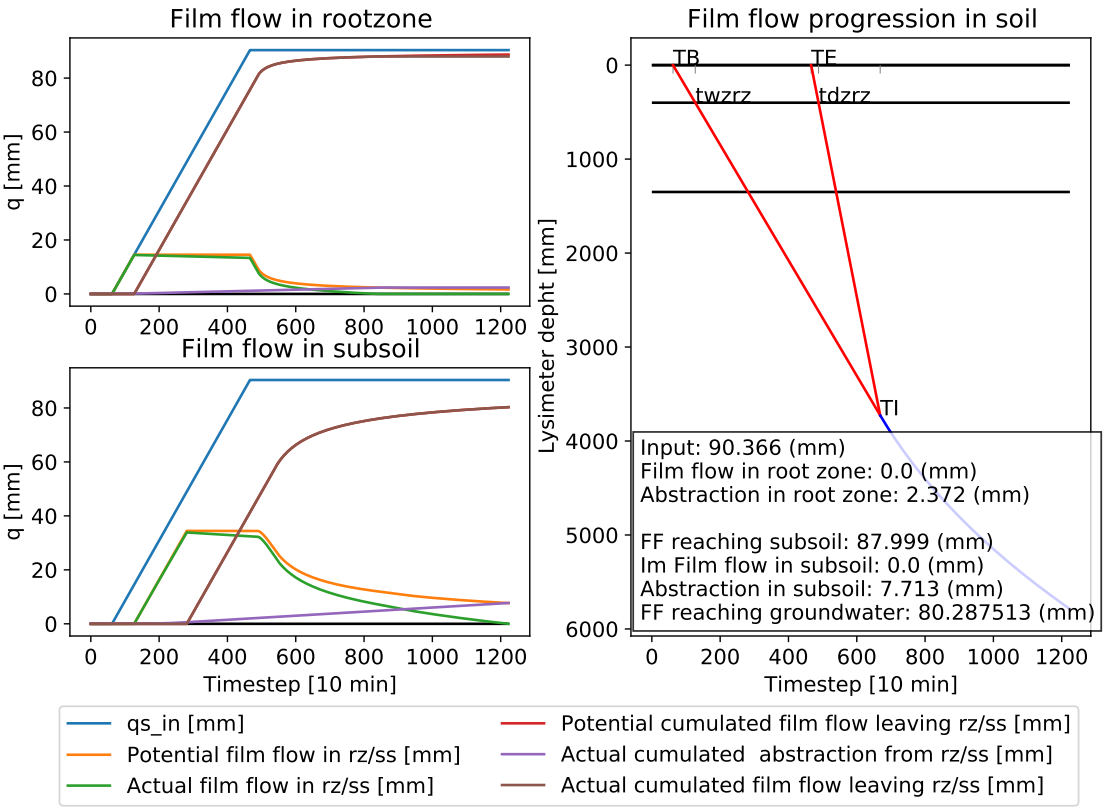

Figure 4.6: Film flow modeling for event 81100 with termination criterion at 1 % and continuous abstraction.

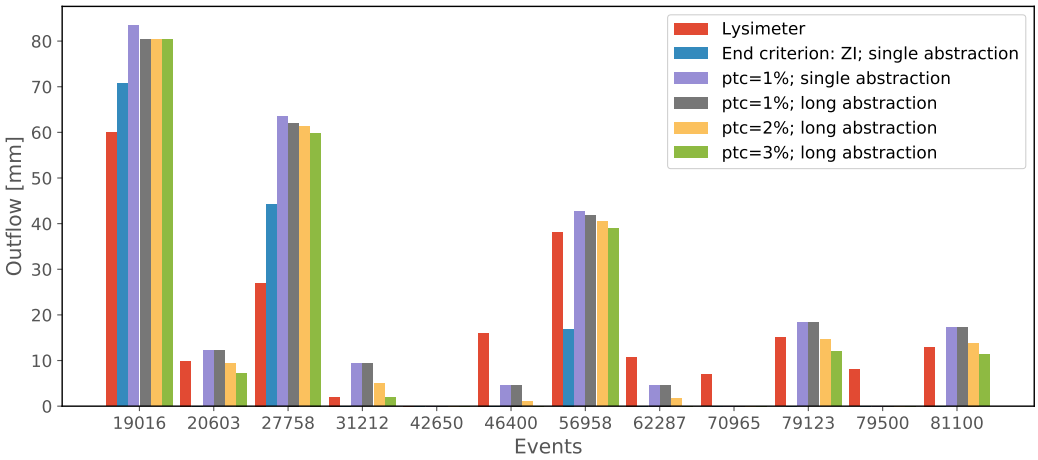

Figure 4.7: Comparison of different models (single or long abstraction) and end criteria (ZI, 1-3% ptc) for different events.

portion. The draining part from the redistribution in the soil is not included. The investigated models differ in their termination criterion and abstraction duration. In the ZI model, the film flow ends at the intersection of the wetting front and drainage front. The abstraction is only calculated at the initial wetting of the macropore wall.

For the other model runs, the abort criterion was calculated using the fraction of water in the film flow. For models marked with *long*, the abstraction is calculated continuously as the wetting front progresses.

Compared to the other model runs, the outflow is lowest for ZI. In 8 out of the 11 cases where the lysimeter shows an outflow, no film flow is calculated by model ZI. The film flow percolation of the other models calculated with the percentage termination criterion all give comparable results. The higher the percentage of the abort criterion is, the more outflow decreases. Event 19016 represents an expection, where the outflow remains constant. The comparison of the abstraction duration in model *1% single* and *1% long*, shows that the outflow remains identical for small events, and for the larger events, the outflow is smaller for *long* abstraction. For two events, 70965 and 79500, an outflow was observed, but not simulated by any of the applied models.

4.5 Film flow implementation in RoGer

The results shown in this section refer to the implementation of the film flow model in the RoGer model. The film flow model was implemented using the single abstraction approach as well as a variable termination criterion determined by the percentage of q_s. If not stated otherwise, the subsequent graphs are based on the same model run, with a termination criterion at 2% of q_s. The model was tested for the entire month of June 2016. Table 4.4 gives a complete list of the used parameters for the model run.

The simulated percolation roughly follows the observed percolation (Fig.4.8). The simulated percolation includes both the film flow component and the drainage component from the subsoil, which results from the redistribution in the soil. Between June 5 and June 21, four percolations events have been recorded. A reaction of the model can be detected in all four events. In the first and third event the simulated outflow is described by the subsoil drainage. For the second and fourth, film flow dominates. In the events that are dominated by the film flow, a temporal offset can be seen. The simulated outflow appears delayed after the observed one. The simulated outflows, which are driven by matrix dominated processes are represented more accurate in time. After June 21, additional outflow events can be seen

Table 4.4: Parameters for the model run.

Unit	No	1
;	lu_id	8
;	trees	0
;	urban	0
[%]	sealing	0
[m/m]	slope	0.01
[mm]	S_tot_dep	0
[mm]	z_soil	1350
[1/m2]	dmpv	100
[mm]	lmpv	600
[1/m2]	dmph	0
[-]	theta_ac	0.12
[-]	theta_ufc	0.15
[-]	theta_pwp	0.2
[mm/h]	ks	1.6
[mm/h]	kf	2500
[-]	a	0.1973
[-]	c	1
[-]	ptc	0.02
[-]	p_weight	1
[-]	ta_weight	1
[-]	et_weight	1

originating from the subsoil drainage. These events are, in this form, not found in the observed data. The course of the simulated volumetric soil water content follows that of the observed values (Fig.4.9). The values in the first half of the modeled time series are better represented than in the second. The values in the first period are slightly underestimated and a temporal delay can be recognized.

The simulated volumetric soil water content for the root zone is strongly underestimated compared to the observed data from the soil depth 10-30 cm (Fig. 4.10). Compared to the simulated data, the observed values are very dynamic and have a larger range.

Figure 4.11 compares the simulated volumetric soil water content of the sub soil with the observed soil water content from 60 -90 cm soil depth. The dynamic of the two curves is similar, with the range of the simulated values being larger than that of the observed values. The volumetric soil water content in the subsoil is to a large extent overestimated by the model.

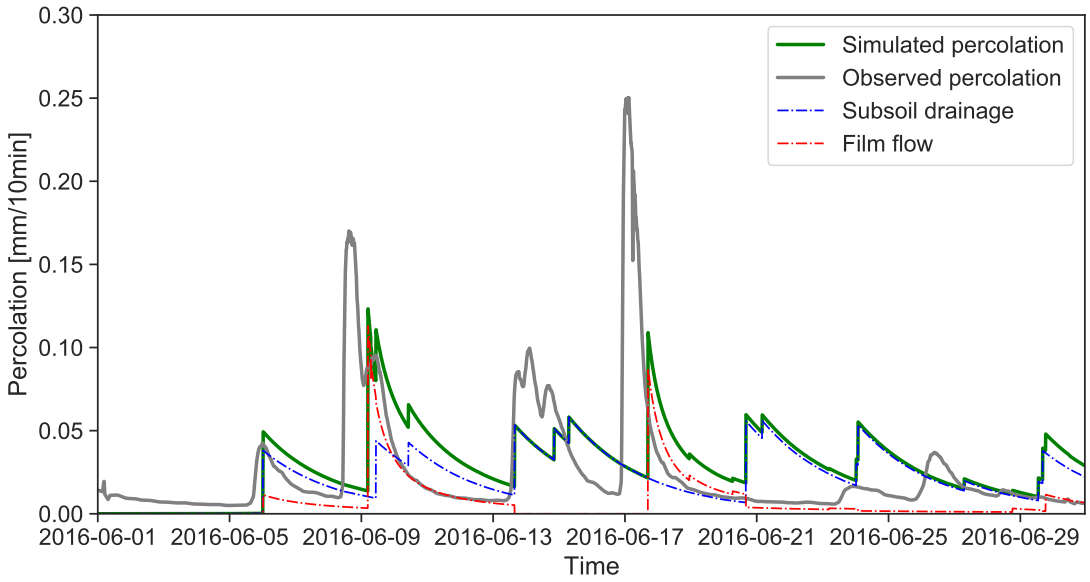

Figure 4.8: Comparison of observed and simulated percolation. Representation of the subsoil drainage and film flow components.

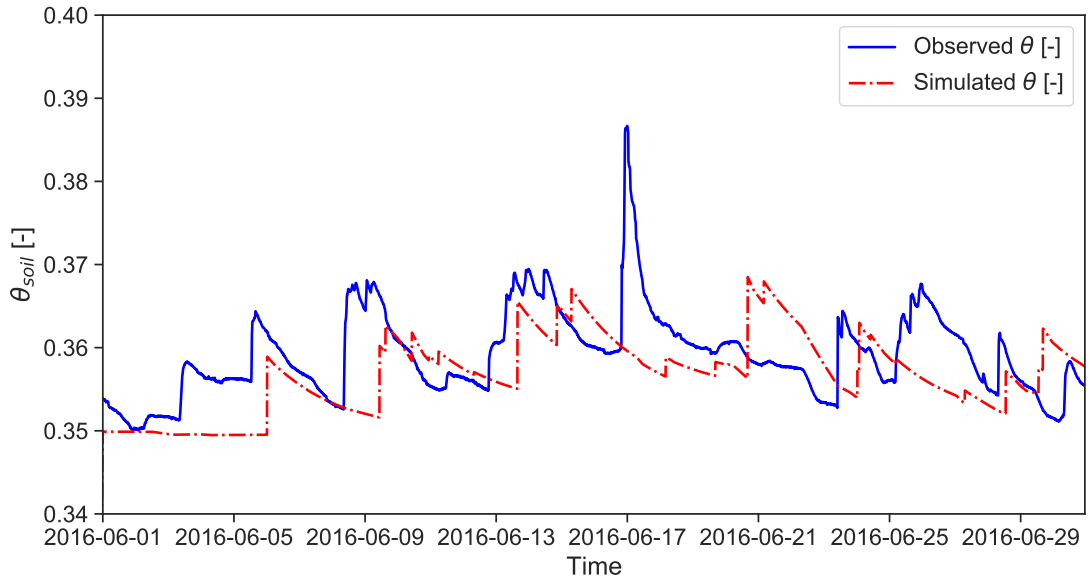

Figure 4.9: Comparison of the observed and the simulated volumetric soil water content averaged over the soil columns.

Figure 4.12 compares the overestimate from the subsoil with the underestimate from the root zone. The overestimation and underestimation complement each other. The range of the underestimation in the root zone is higher than the range of the overestimation in the subsoil.

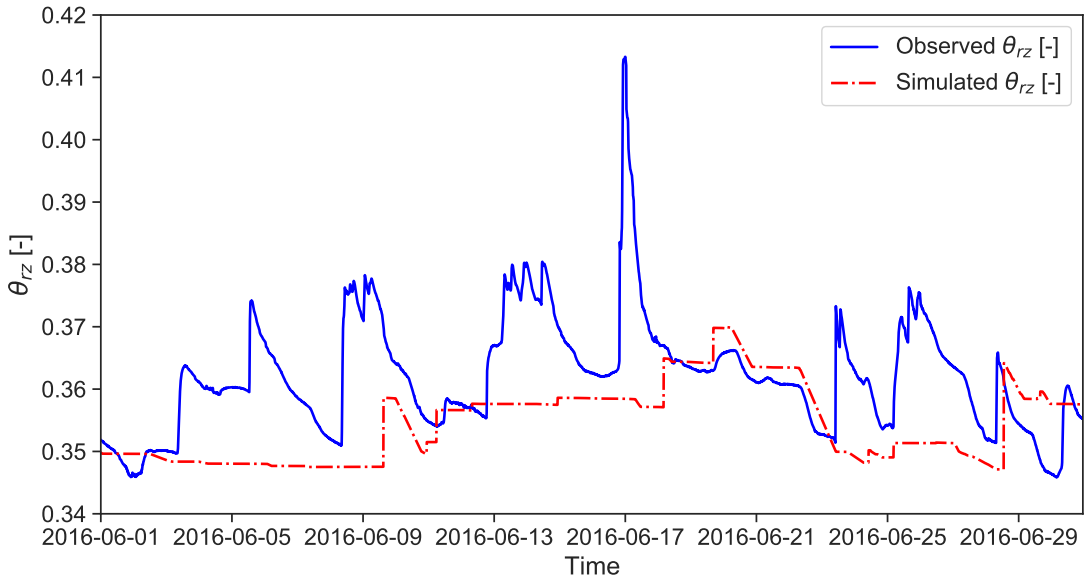

Figure 4.10: Comparison of the observed and the simulated volumetric soil water content of the root zone.

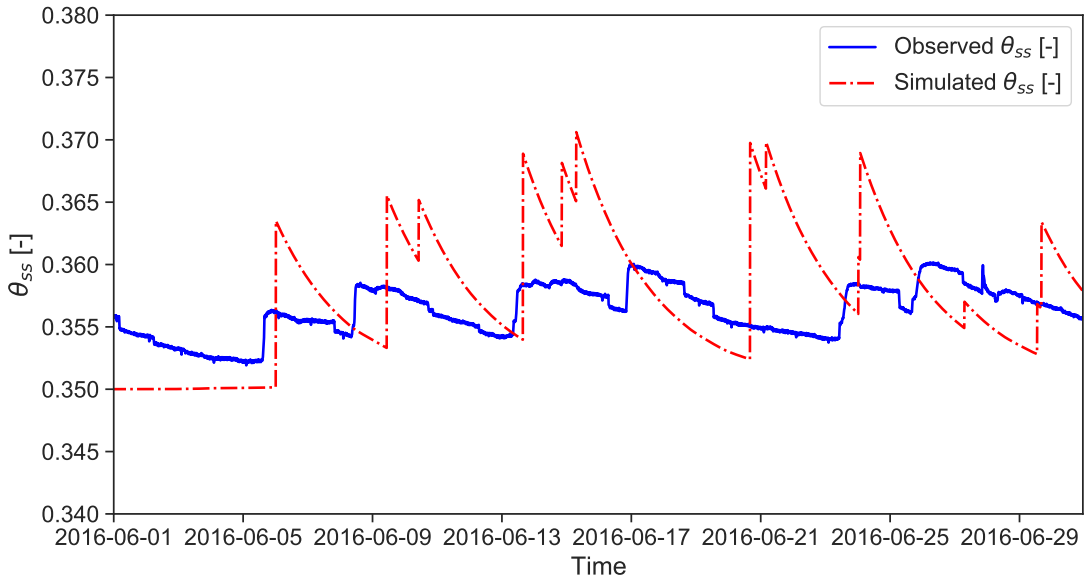

Figure 4.11: Comparison of the observed and the simulated volumetric soil water content of the subsoil.

Figure 4.13 and 4.14 show the volumetric soil water content of the root zone and the subsoil, including the water content in the film flow. In the root zone, the volumetric water content remains unchanged. In the subsoil, the simulated volumetric water content with film flow is higher than the observed volumetric water content.

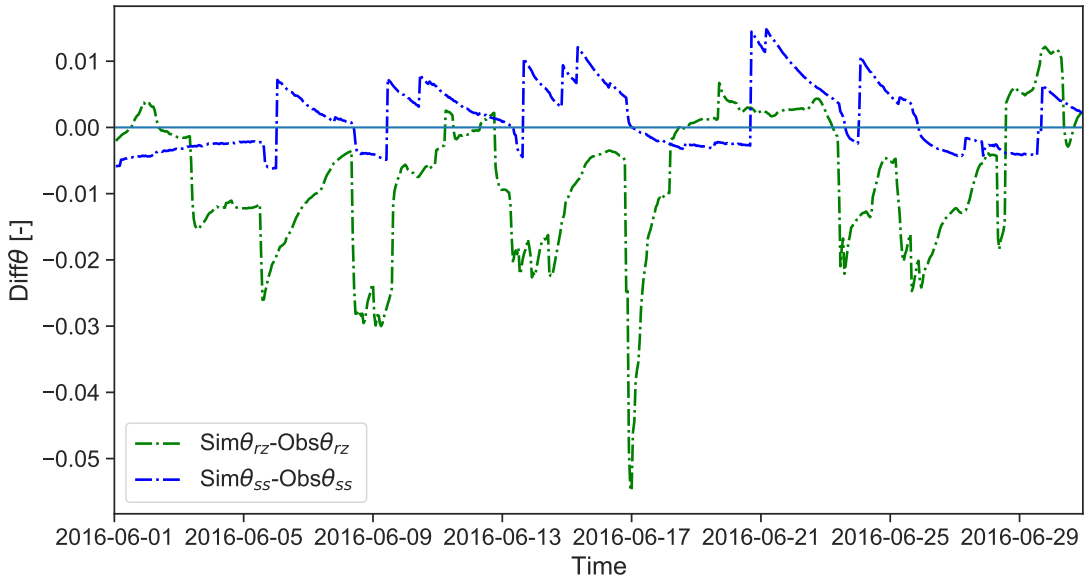

Figure 4.12: Comparison of the overestimation form the subsoil and the underestimation from the root zone.

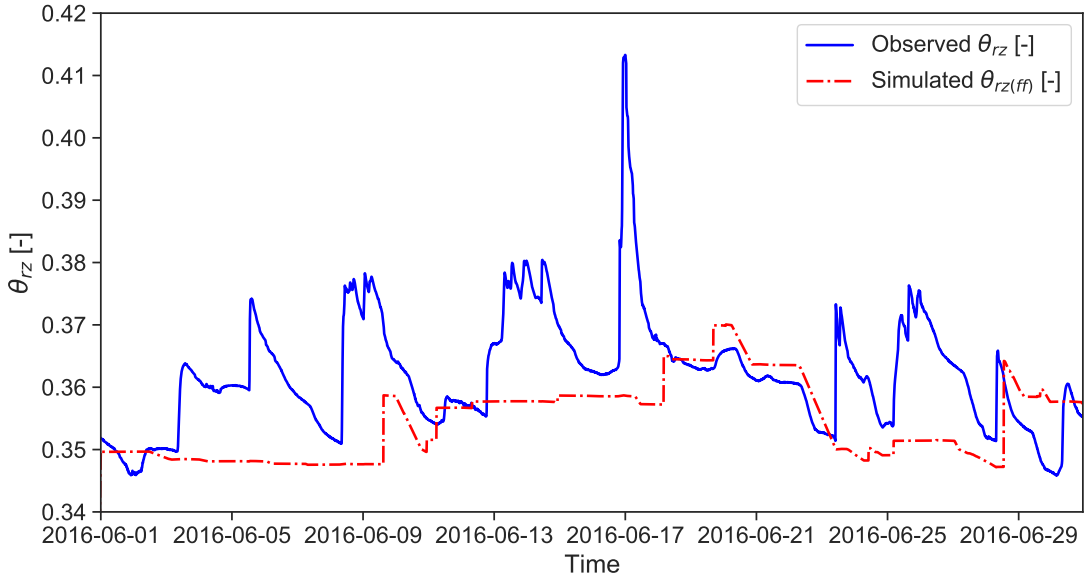

Figure 4.13: Comparison of the observed and the simulated volumetric soil water content of the root zone, including the water from the film flow.

The figure 4.15 shows the residual film flow, which remains in the preferential flow paths and is not directly abstracted. At the end of a film flow event defined by the abort criterion, the remaining film flow is abstracted into the ground. A decrease in residual film flow results in an increase in water content in either the root zone or the subsoil. The abstraction is simulated fractionally. A high abstraction can

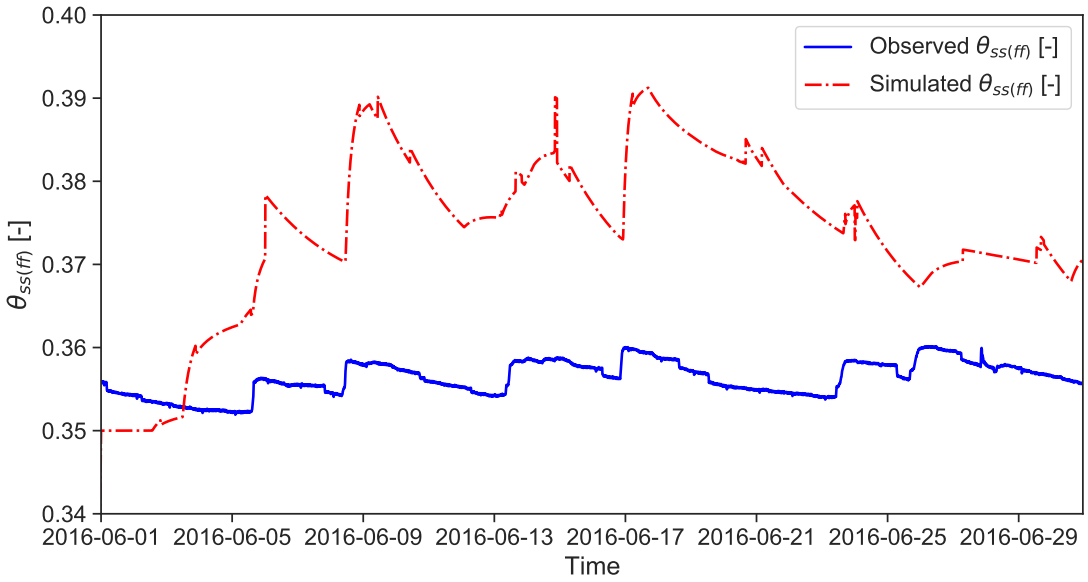

Figure 4.14: Comparison of the observed and the simulated volumetric soil water content of the subsoil, including the water from the film flow.

only be recognized for single time steps. The abstraction into the root zone or the subsoil leads to an increase of the soil water content in the respective soil layer as shown in figure 4.16.

In the top portion of figure 4.17, the observed precipitation is shown in red. The input pulse, which is used to model the film flow, is shown in blue. The wetting front and drainage front of each event for the given input pulse are shown in the middle portion of figure 4.17. The wetting fronts of events #3, #14, #22, #24 and #31 reach a depth of 1350 mm and thus reach the groundwater. Events #22 and #24 have a long tailing and barely leave the bottom layer. In the lower portion of figure 4.17, three of the above-mentioned events (#3, #14 and #31) contribute to direct groundwater recharge. Compared to the observed percolation, the film flow is delayed.

In the graphs 4.18 and 4.19, one input parameter was changed in RoGeR. In the initial classification of the events in RoGeR, the time span of a precipitation-free period, which separates two events from each other, was extended from 2 hours to 4 hours. In the figure 4.19 this change of the parameter, results in a different classification of the events. Compared to figure 4.17, fewer events are modeled. The film flow for Event #13 (Fig. 4.19) is more significant than for the comparable Event #31 from Figure 4.17.

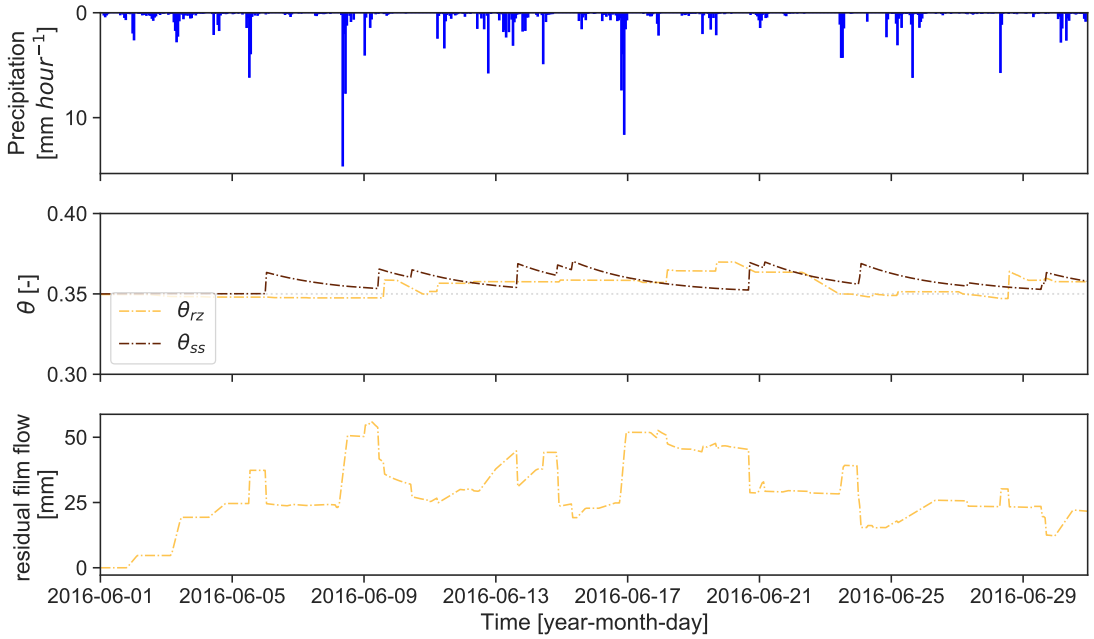

Figure 4.15: Raw precipitation data during month June 2016 (top), simulated volumetric soil water content for the root zone and subsoil (center), residual film flow(bottom).

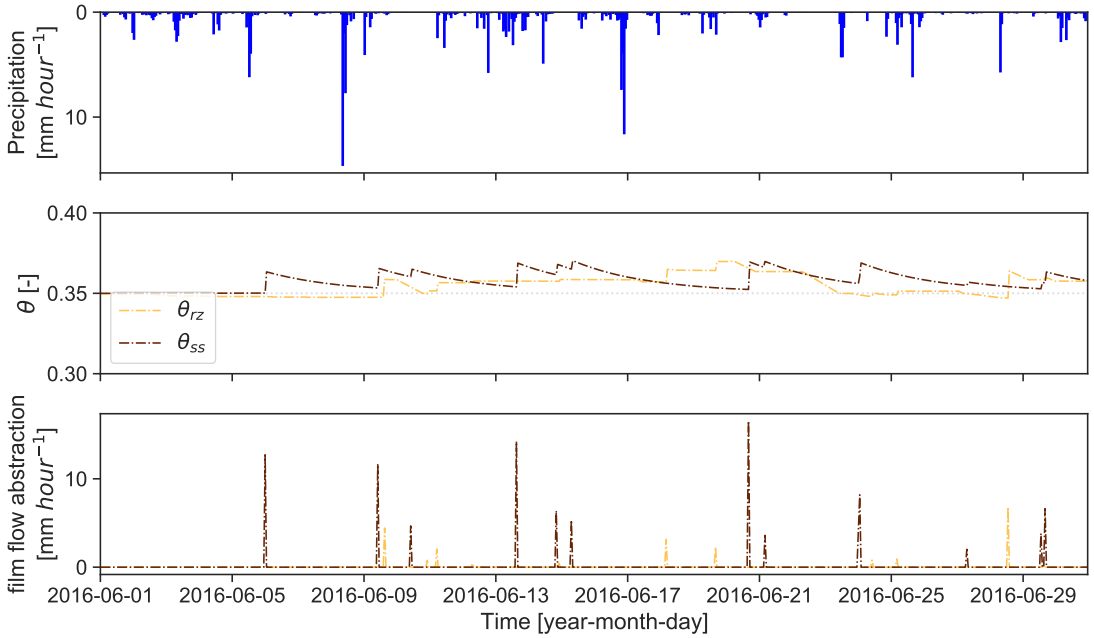

Figure 4.16: Raw precipitation data during month June 2016 (top), simulated volumetric soil water content for the root zone and subsoil (center), abstraction from film flow into root zone and subsoil including residual water content (bottom).

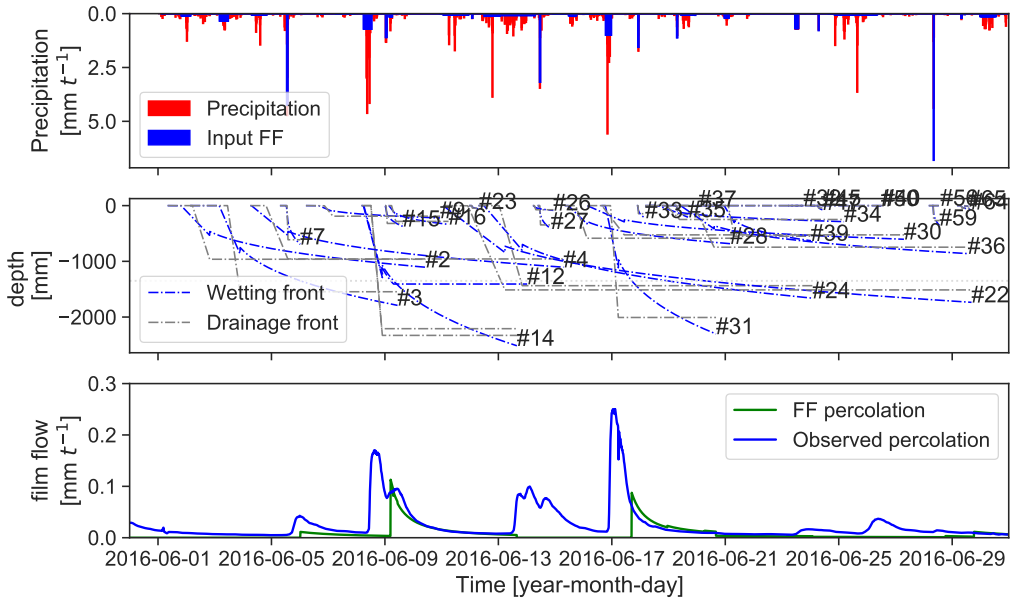

Figure 4.17: Raw precipitation data and input pulse forming the film flow(top), propagation of the wetting and drainage front in the soil(center), observed percolation from the lysimeter and simulated actual film flow (bottom).

Figure 4.21 compares different classifications of precipitation events. For this purpose, the parameter *end_of_p_event* in RoGeR was changed. The parameter *end_of_p_event* gives the maximum precipitation-free period until a new event is defined. This is decisive for the classification of the rain events. 2- and 4-hour precipitation-free durations were compared. Given a 2 hour timespan a larger number of film flow events is generated (Fig.4.17). Comparing the two main events in the upper graph of figure 4.21, Comparing the two main events in the upper graph of figure. In one event the maximum intensity of the film flow decreases and in the other it increases. Same with the arrival time, at the first major event the film flow arrives late with an end of event duration of 4 hours and at the second major event the film flow arrives early compared to simulation with the 2 hours end of event time. With an end of event duration of 4 hours, a new film flow event breakthrough appears on June 5. In the lower graph of the same figure the simulated percolation is compared with the observed one. With an end of event length of 4 hours, the event on June 17 is better represented, both in terms of time and intensity. The new appearing event simulated on June 5 is not reflected in the observed data.

The figure 4.22 illustrates different termination criteria. The upper graph shows the film flow portion of the percolation. With a ptc value of 0.02, the film flow

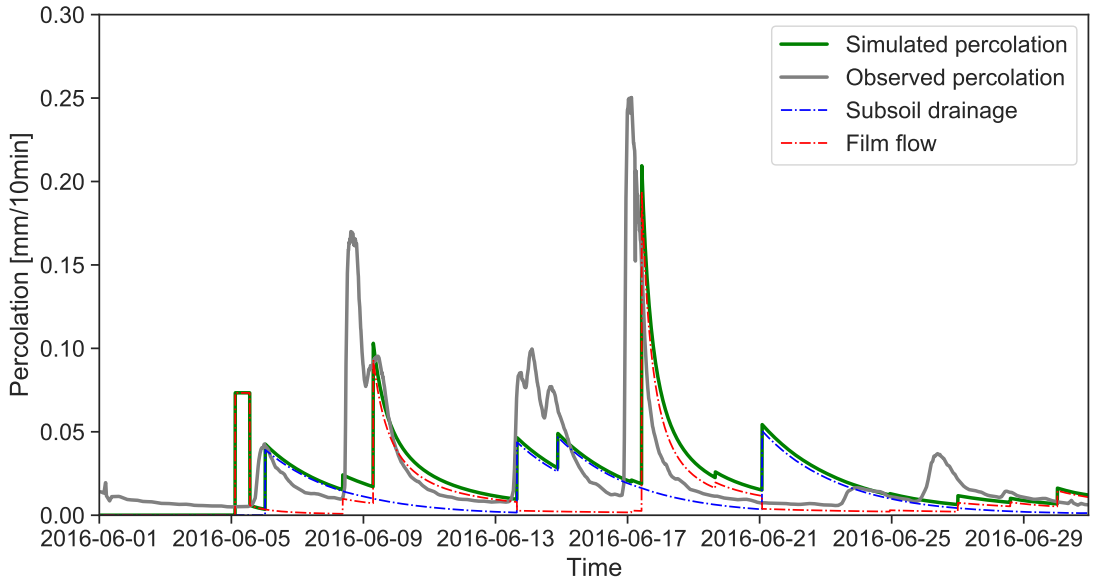

Figure 4.18: Comparison of observed and simulated percolation with *end_of_event* =24. Representation of the subsoil drainage and film flow components.

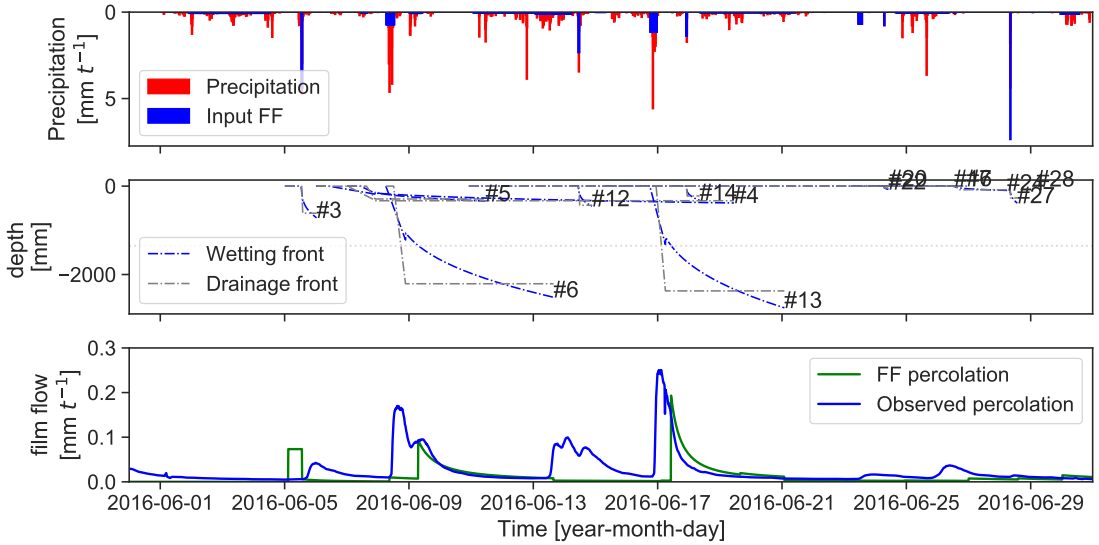

Figure 4.19: Raw precipitation data and input pulse forming the film flow(top), propagation oft the wetting and drainage front in the soil(center), observed percolation from the lysimeter and simulated actual film flow (bottom); [*end_of_event* =24].

contributes most to the percolation. There are 4 film flow peaks with a long tailing. At a ptc value of 0.10, 2 peaks are detectable. The tailing of the peaks is reduced and there is an abrupt end to the film flow. The initial intensity of the film flow of both peaks is the same as for the matched events with a ptc value of 0.02. The

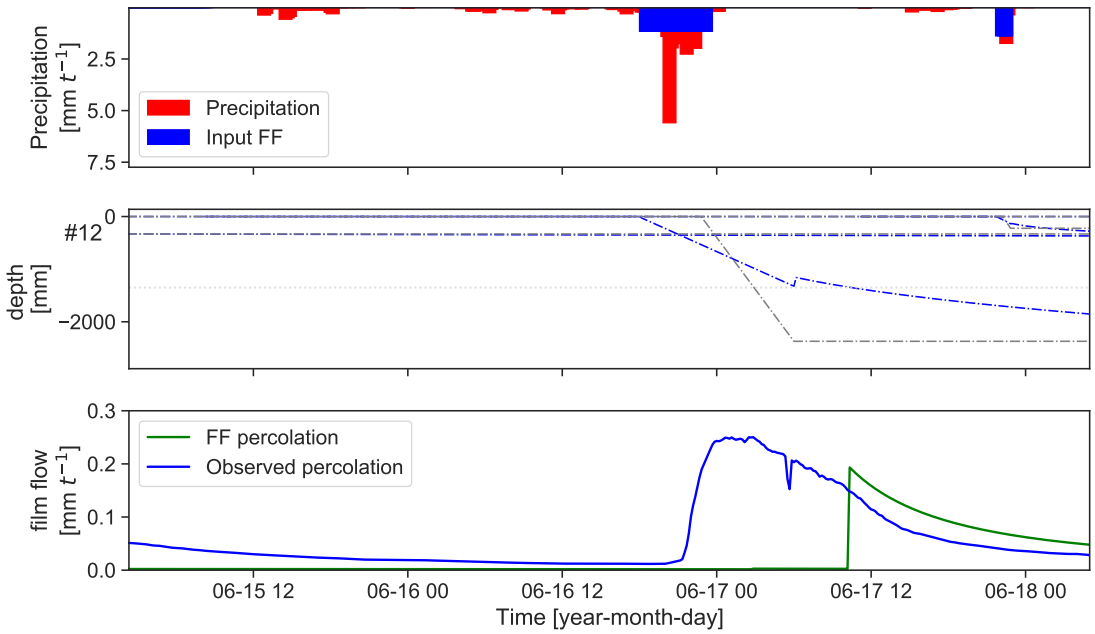

Figure 4.20: Detail: Raw precipitation data and input pulse forming the film flow(top), propagation of the wetting and drainage front in the soil(center), observed percolation from the lysimeter and simulated actual film flow (bottom); [end_of_event =24].

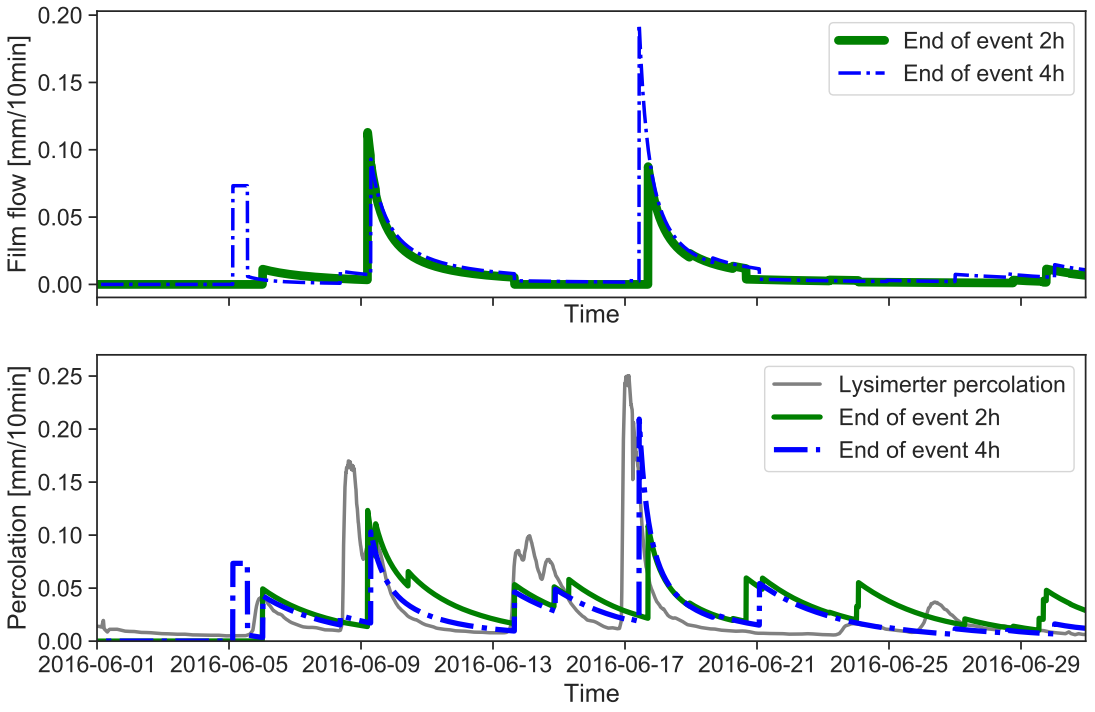

Figure 4.21: Comparison of film flow (top) and drainage (bottom) for different $end\_of\_p\_event$.

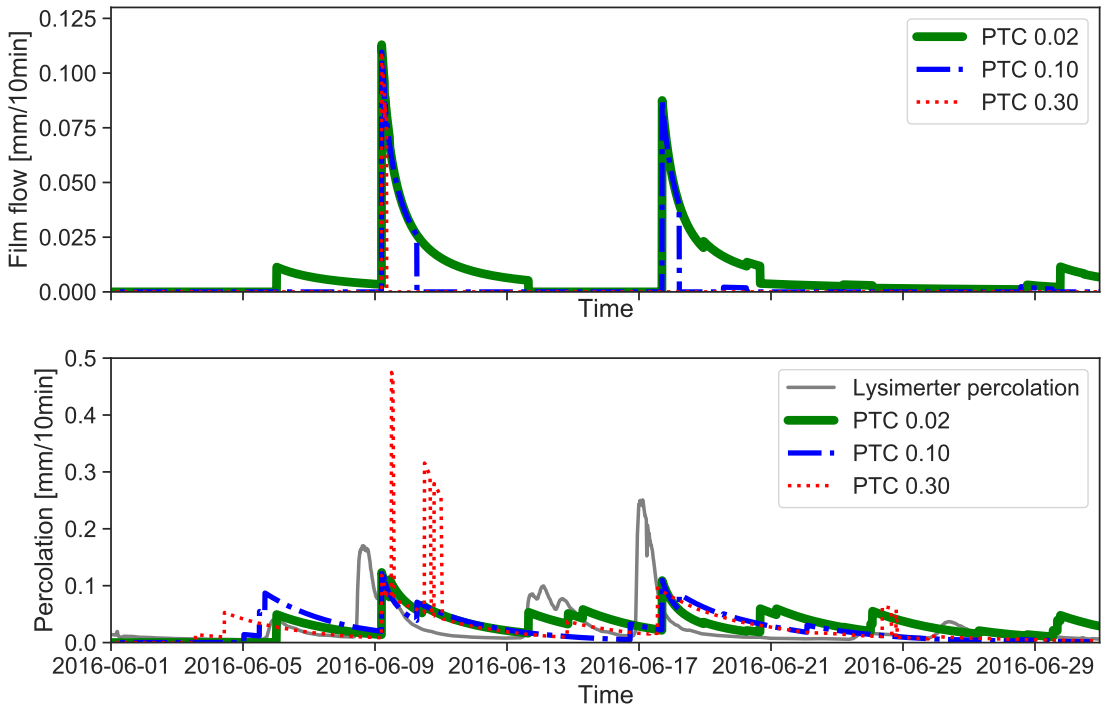

Figure 4.22: Comparison of film flow (top) and drainage (bottom) for different ptc values.

initial intensity of the film flow of both peaks is comparable to the matched events with a ptc value of 0.02. With a ptc value of 0.3 the film flow component reaches the groundwater in only one measurement. The bottom graph at the bottom compares the total percolation for different ptc values. The simulation with a ptc value of 0.02 is closest to the observed percolation values. For the event on June 5, 2016, the percolation for the higher ptc values takes place earlier. For the values 0.10 and 0.30 no percolation is modeled on June 13 and 17. The modeling with the ptc value at 0.30 results to a certain extent in very high percolations shortly after June 9.

5 Discussion

5.1 Defining the input pulse

Finding events in the time series where the increase in volumetric soil water content was clearly defined at all depths was difficult. The coefficient of determination of the linear regression of depth and arrival of the wetting front shows that the flow velocity for some events can be considered constant. For two of the selected events, the coefficient of determination indicates a poorer fit of the linear regression. This is because the wetting front arrives earlier at a depth of 60 cm than at a depth of 30 cm. One possible explanation would be that there is probably a preferential flow path that passes by the FDR probe at 30 cm. The FDR sensor does not cover the complete cross section of the lysimeter. Therefore, it is possible that preferential flow was not detected. The magnitude of the determined flow velocities is comparable to that of other studies (Demand and Weiler 2021, Germann and Prasuhn 2018).

The parameters of the input pulse were determined with a method developed by Demand and Weiler 2021. The evaluation of this approach for different events has revealed large differences between the observed and modeled start and end points 4.2. Considering the two examples in figure 4.2, it can be argued, that if TB>tb, the low intensity at the beginning of the event does not lead to the formation of film flow. Conversely, if TB<tb, the film flow is modeled too early. In almost all cases, TE is modeled too early. This leads to a shortened modeling of the film flow event. The drainage front catches the wetting front at an earlier time. The shift of the end point is not as severe as the shift of the start point. This is because the end point is set so that the input pulse is equal to the cumulative observed rainfall and is dependent on the volume flux density. The parameter TB indicates the starting point of the film flow and specifies when the precipitation enters the soil.

It should be noted that events with longer precipitation-free periods were also considered in the evaluation. The slight correlation between the maximum percolation-

free time during an event and the deviation of the starting point confirms that heterogeneous events are mapped worse in time. This point will be discussed further in section 5.5.

More important than the timing of the input pulse, is that that the water balance is correct, and that the cumulative precipitation is properly represented in the pulse. The comparison of the modeled and observed cumulative precipitation pulses shows deviations in the decimals. This is because the modeled starting point TB was rounded and so the interval of the pulse has an incorrect length. Because the model works with discrete time steps this problem cannot always be avoided later in the model. An example of this are the jumps seen in the modeling of the wetting front in (Fig.4.20).

5.2 Parameterization of the film flow process

The initial fit of the linear regression between the precipitation intensity and the manually calculated film flow velocity gives a parameter b of 0.607 which is only slightly lower than the ideal exponent 2/3. The hypothesis that the film flow is modeled by the kinematic wave theory can thus be accepted (Germann and Karlen 2016). The significance of the obtained exponent, can be explained by the fact that the experimental setup uses a lysimeter and that vegetation has no disturbing influence on the infiltration of the measured precipitation. Demand and Weiler (2021) have found that parameter b is closest to the ideal value of 2/3 for grassland vegetation.

5.3 Abstraction

The abstraction describes the process of horizontal infiltration from the macropores into the surrounding soil matrix. In this study, different approaches describing abstraction were investigated. The goal was to describe the abstraction using a physics-based approach and as few parameters as possible. In addition, the conditions of the film flow had not to be violated.

5.3.1 Abstraction time

One hypothesis made at the beginning was that the abstraction only occurs at the initial wetting of the macropore wall. This assumption was made because the advancement of the wetting and drainage fronts are directly related to volume flux density. If too much water were removed from the film flow, this relationship would no longer be true, and one could no longer assume a constant flow velocity during an event. A second reason why this assumption was made is that we did not assume pore geometry. The wetting fronts of the horizontal matrix infiltration meet at a certain point in time, which leads to a termination of the infiltration since the wetting front suction approaches zero.

The experiments with the single event approach have shown that the direct horizontal abstraction is minimal (Fig. 4.5). Continuous abstraction was also modeled for the same events. With continuous abstraction, the share of direct abstraction for the event is 14% of the input. From a physical point of view, it is more likely that water will continue to abstract from the film flow into the soil matrix after the first wetting. Steinbrich et al. (2016) shortend the acitve length of the macropore by the arrival of the wetting front of the vertical matrix infiltration. Limiting the continuous/long abstraction to the arrival of the drainage front in the film flow model could be considered as a similar approch, that should be evaluated.

5.3.2 Abstraction of the residual film flow

As can be seen in the single event attempts, a residual film flow remains after the end of the film flow event. This part must also be added to the soil. For the single event modeling no solution for this problem was implemented. It is assumed that the water remains in the layer in which it is located. However, when implemented in Roger, concrete framework conditions, that clearly define the storage into which the water from the residual film flow will be absorbed, must be garanteed.

The assumption made in the RoGeR model is that all the remaining film flow from both soil layers abstracts into the soil layer where the wetting front is located at the end of the film flow. This means that if the film flow ends in the root zone, the residual film flow will be abstracted in addition to the direct abstraction in the root

zone. If the film flow continues into the subsoil, the residual film flow is abstracted at the end of the film flow in the sub soil.

This approach contradicts the direct abstraction. The absorption capacity of the soil matrix is limited and should be completely utilized during the direct horizontal abstraction from the film flow. An additional abstraction of the residual film flow at the end of the film flow into the soil matrix would not be possible because the absorption capacity of the soil is limited.

The rest of the film flow is abstracted at the end of the film flow in the last time step of the event. This leads to the single peaks with very high abstraction rates as shown in figure 4.16. The fact that the main part of the film flow is abstracted only in a single time step at the end of each event, leads to a delayed modeling of the soil water content. The curve resulting from the modeling of soil water content is therefore less detailed and finer processes are not recognizable (Fig.4.11). Considering the proportionally large share of residual film flow that is additionally abstracted at the end of the film flow, the approach to abstraction (3.1.5) must be considered with caution, even if the figure 3.1 shows that the simulated volumetric soil water content is within good agreement with the observed.

The volumetric soil water content is underestimated in the root zone and overestimated in the subsoil (Fig.4.12). Since the main part of the abstraction consists of the residual film flow added to the bottom matrix at the end of the film flow, the error leading to these deviations is most likely to occur here. One possible explanation for this would be that the water in the film flow is abstracted to only one of the two soil layers as explained at the beginning of this section. A better approach would be to consider the residual film flow for each layer individually and abstract it in each respective soil layer. This would however not solve the problem that more water is abstracted than specified by the original direct abstraction.

5.4 End criterion

The termination criterion of the film flow was introduced because the volume flux density converges asymptotically to zero and the film flow process must stop at a certain point for computational reasons. The effects of the different abort criterion

were tested using both the single event approach and the implementation in the RoGeR model.

The evaluations from the single event approach show that a termination at ZI produces inferior results. A termination of the film flow at ZI means that the film flow does not contribute to groundwater recharge in most of the events examined. When evaluating the single event approach, it should be noted that the modeled film flow cannot be directly compared with the observed percolation from the lysimeter. A direct comparison would only be possible if the percolation from the redistribution in the soil matrix were also considered. However, this was not done for the single event approach.

By including the film flow approach in the RoGeR model a comparison between the percolation of the model and the percolation of the lysimeter becomes possible. Figure 4.22 shows that the ptc parameter causes the film flow process to break, but not change the shape or temporal position of the existing peaks. Earlier cessation of the film flow led to a different redistribution in the soil. The residual film flow is abstracted into the ground earlier. Because there is less water in the film flow, the volumetric soil water content of the soil matrix is higher.

A phenomenon that can happen with an early termination of the film flow is that the simulated percolation occurs before the observed one. This can be seen in the figure 4.22 on the 5^{th} of June. This is because the residual film flow includes the film flow of both layers. If the film flow only just reaches the subsoil layer, all the water of the film flow is abstracted at once. Because the subsoil is considered as one layer, the volumetric water content rises and the drainage, from the subsoil into the groundwater, starts. This would be partly avoidable if the residual film flow were distributed to the root zone and subsoil, as explained in the section 5.3.2.

The parameter ptc shifts the time of abstraction of the residual film flow. It can be argued that a longer tailing of the film flow event, i.e. a smaller ptc value, better reflects the distribution of the water in the soil. The percolating film flow was best represented with a ptc value of 0.02. Very high single-amount abstractions and an early breakthrough into the groundwater can be prevented in this way.

Demand and Weiler (2021) introduced the termination criterion based on the decline of mobile water content w. The parameter S describes the decline of the mobile water content as portion of the $w(F, L)$. The best overall decline parameter

S_{opt} is 0.26. This confirms, that ZI cannot be used as a termination criterion.

Germann and Beven (1985) limited the the macropore flow to the point where all water is absorbed by the soil matrix.

5.5 Event classification

Based on precipitation input data, event classification is performed in advance. The parameter *end_of_p_event* controls how long an event persists after the end of the observed precipitation. In other words, the parameter describes how long a precipitation-free period can remain within an event. By default, the value is set to 12 times 10 minutes, i.e. 2 hours. With smaller *end_of_p_event* values, several shorter events are generated over the modeled period. For larger *end_of_p_event*, multiple precipitation periods are combined into one larger event. The parameter *end_of_p_event*, therefore has a great impact on the modeling of the film flow.

In figure 4.19 for larger *end_of_p_event* several smaller events are merged. . This leads to the input pulse having a low intensity but is being very wide. The film flow reaches greater depths because it takes time for the drainage front to catch up with the wetting front. The first input pulse in the figure, for example, lasts for more than three days.

At the June 17 event (Fig.4.21), an end-of-event better models the film flow. Firstly, the wetting front arrives earlier at the bottom of the groundwater and secondly, the volume flux density corresponds more closely to the observed volume flux density. It is not possible to make a general statement as to whether the end of event parameter should be smaller or larger. An argument for a smaller end of event parameter can be found in the results of section 4.2. Here, a correlation between the deviation of the input pulse and the precipitation-free periods within an event is shown. Smaller values lead to a greater number of small events, which lead to less variability within the events. This is then beneficial for the method of determining the input pulse (3.1.2).

In addition to the existing parameter (*end_of_p_event*) of event classification, a parameter could be introduced to determine the intensity at which film flow occurs. This could, in theory, prevent very long events with low intensity from leading to

film flow.

Another approach in contrast to a homogeneous input pulse for an event, would be several pulses varying in intensity for an event. This is described by Germann (2014) as superposition of kinematic waves. The approach would help to better represent larger events with varying intensities as not only one consitant volume flux density has to assumed. However this approach requires even more effort to keep track of the wetting fronts of the indivudual subevents.

5.6 Implementation of overlapping events

The overlapping wetting fronts of the events posed a challenge to the implementation of the film flow in a hydrological model RoGeR. Modeling two wetting fronts at the same time would involve a large computational effort. This problem was solved well by calculating the film flow events completely in advance. However, this approach is only practicable for small time series, since for longer time series this approach would increase the modeling time signifcantly.

6 Conclusion

The results of this study confirm the relationship between the input pulse and film flow velocity. The method for determining the input pulse shows major differences between the simulated and observed start and end points. The initial classification of events plays a major role in the formation of film flow as it influences the number, the position and volume flux density of the input pulses. An additional parameter that determines the precipitation intensity at which preferential flow occurs could be introduced to further classify events. The modeling of abstraction remains a challenge. The physics-based abstraction equation proposed in this study, results in very small abstraction values that are not sufficiently large enough to explain the abstraction of the residual film flow. A different approach is needed, preferably with no residual film flow remaining in the soil layers after the end of the event. With a very small abstraction rate, a continuous abstraction into the soil matrix can be assumed. A reason for this is that low abstraction has no influence on the speed of the wetting front. The end criterion is decisive for how deep the film flow process can progress into the soil and influences heavily the water redistribution. Optimal model results were obtained with a late termination of the film flow. The assumption that the film flow after ZI no longer needs to be considered, can be rejected. Despite the overlapping wetting fronts of the individual events, it was possible to integrate the film flow into the hydrological model RoGeR using a simple analytical approach. A next step would be a sensitivity analysisto further hone down on the different values of the parameters. In conclusion, it can be said that the film flow could be integrated into the hydrological model RoGeR and significant results were obtained. The abstraction remains the biggest difficulty and needs further improvement.

References

Beven, K. and Germann, P. (1981). "Water Flow in Soil Macropores Ii. a Combined Flow Model". In: *Journal of Soil Science* 32.1, pp. 15–29. DOI: 10.1111/j.1365-2389.1981.tb01682.x.

Beven, K. and Germann, P. (Oct. 1982). "Macropores and water flow in soils". In: *Water Resources Research* 18.5, pp. 1311–1325. DOI: 10.1029/WR018i005p01311.

Beven, K. and Germann, P. (June 2013). "Macropores and water flow in soils revisited: REVIEW". In: *Water Resources Research* 49.6, pp. 3071–3092. DOI: 10.1002/wrcr.20156.

Bormann, H. and Klaassen, K. (June 2008). "Seasonal and land use dependent variability of soil hydraulic and soil hydrological properties of two Northern German soils". In: *Geoderma* 145.3, pp. 295–302. DOI: 10.1016/j.geoderma.2008.03.017.

Brooks, R. H. and Corey, A. T. (1964). "HYDRAULIC PROPERTIES OF POROUS MEDIA". In: *Hydrology Papers Colorado State University*, p. 37.

Bundt, M., Widmer, F., Pesaro, M., Zeyer, J., and Blaser, P. (May 2001). "Preferential flow paths: biological 'hot spots' in soils". In: *Soil Biology and Biochemistry* 33.6, pp. 729–738. DOI: 10.1016/S0038-0717(00)00218-2.

Coppola, A., Kutílek, M., and Frind, E. (Feb. 2009). "Transport in preferential flow domains of the soil porous system: Measurement, interpretation, modelling, and upscaling". In: *Journal of Contaminant Hydrology* 104.1, pp. 1–3. DOI: 10.1016/j.jconhyd.2008.05.011.

Darcy, H. (1856). *Les fontaines publiques de la ville de Dijon: exposition et application ...* Google-Books-ID: DOwbgyt_MzQC. Victor Dalmont. 666 pp.

Demand, D. and Weiler, M. (May 2021). "Potential of a Gravity-Driven Film Flow Model to Predict Infiltration in a Catchment for Diverse Soil and Land Cover Combinations". In: *Water Resources Research* 57.5. DOI: 10.1029/2019WR026988.

Djodjic, F., Börling, K., and Bergström, L. (Mar. 2004). "Phosphorus Leaching in Relation to Soil Type and Soil Phosphorus Content". In: *Journal of Environmental Quality* 33.2, pp. 678–684. DOI: 10.2134/jeq2004.6780.

Flury, M. (Jan. 1996). "Experimental Evidence of Transport of Pesticides through Field Soils—A Review". In: *Journal of Environmental Quality* 25.1, pp. 25–45. DOI: 10.2134/jeq1996.00472425002500010005x.

Gerke, H. H. and van Genuchten, M. T. (Feb. 1993). "A dual-porosity model for simulating the preferential movement of water and solutes in structured porous media". In: *Water Resources Research* 29.2, pp. 305–319. DOI: 10.1029/92WR02339.

Germann, P. and Beven, K. (1985). "Kinematic Wave Approximation to Infiltration Into Soils With Sorbing Macropores". In: *undefined*.

Germann, P. (2014). *Preferential Flow – Stokes Approach to Infiltration and Drainage*. CH: Geographica Bernensia.

Germann, P., Helbling, A., and Vadilonga, T. (May 2007). "Rivulet Approach to Rates of Preferential Infiltration". In: *Vadose Zone Journal* 6.2, pp. 207–220. DOI: 10.2136/vzj2006.0115.

Germann, P. and Prasuhn, V. (2018). "Viscous Flow Approach to Rapid Infiltration and Drainage in a Weighing Lysimeter". In: *Vadose zone journal* 17.1. In collab. with P. Germann and V. Prasuhn. Number: 1 Publisher: Soil Science Society of America SSSA. DOI: 10.2136/vzj2017.01.0020.

Germann, P. F. (2017). "Shape of Time Domain Reflectometry Signals during the Passing of Wetting Fronts". In: *Vadose Zone Journal* 16.2, vzj2016.08.0070. DOI: 10.2136/vzj2016.08.0070.

Germann, P. F. and Di Pietro, L. (May 1999). "Scales and dimensions of momentum dissipation during preferential flow in soils". In: *Water Resources Research* 35.5, pp. 1443–1454. DOI: 10.1029/1998WR900112.

Germann, P. F. and Karlen, M. (Feb. 2016). "Viscous-Flow Approach to In Situ Infiltration and In Vitro Saturated Hydraulic Conductivity Determination". In: *Vadose Zone Journal* 15.2, vzj2015.05.0065. DOI: 10.2136/vzj2015.05.0065.

Germann, Peter (1985). "Kinematic Wave Approach to Infiltration and Drainage into and from Soil Macropores". In: *Transactions of the ASAE* 28.3, pp. 745–749. DOI: 10.13031/2013.32331.

Hagedorn, F. and Bundt, M. (July 1, 2002). "The age of preferential flow paths". In: *Geoderma* 108.1, pp. 119–132. DOI: 10.1016/S0016-7061(02)00129-5.

Heber Green, W. and Ampt, G. A. (May 1911). "Studies on Soil Phyics." In: *The Journal of Agricultural Science* 4.1, pp. 1–24. DOI: 10.1017/S0021859600001441.

Hincapié, I. and Germann, P. F. (Feb. 2009a). "Impact of initial and boundary conditions on preferential flow". In: *Journal of Contaminant Hydrology* 104.1, pp. 67–73. DOI: 10.1016/j.jconhyd.2008.10.001.

Hincapié, I. A. and Germann, P. F. (Nov. 2009b). "Abstraction from Infiltrating Water Content Waves during Weak Viscous Flows". In: *Vadose Zone Journal* 8.4, pp. 996–1003. DOI: 10.2136/vzj2009.0012.

Jarvis, N. J. (June 2007). "A review of non-equilibrium water flow and solute transport in soil macropores: principles, controlling factors and consequences for water quality". In: *European Journal of Soil Science* 58.3. Place: Hoboken Publisher: Wiley WOS:000246427800001, pp. 523–546. DOI: 10.1111/j.1365-2389.2007.00915.x.

Kung, K.-J. (Mar. 1990). "Preferential flow in a sandy vadose zone: 2. Mechanism and implications". In: *Geoderma* 46.1, pp. 59–71. DOI: 10.1016/0016-7061(90)90007-V.

Lighthill, M. J. and Whitham, G. B. (May 10, 1955). "On kinematic waves II. A theory of traffic flow on long crowded roads". In: *Proceedings of the Royal Society of London. Series A. Mathematical and Physical Sciences* 229.1178. Publisher: Royal Society, pp. 317–345. DOI: 10.1098/rspa.1955.0089.

Prasuhn, V., Spiess, E., and Seyfarth, M. (2009). "Die neue Lysimeteranlage Zürich-Reckenholz". In: 13. Grumpensteiner Lysimetertagung, p. 6.

Richards, L. A. (Nov. 1931). "CAPILLARY CONDUCTION OF LIQUIDS THROUGH POROUS MEDIUMS". In: *Physics* 1.5, pp. 318–333. DOI: 10.1063/1.1745010.

Schwemmle, R. (2021). "RoGeR". In: *GitHub repository*. https://github.com/schwemro/RoGeR/tree/film_flow.

Šimůnek, J., Jarvis, N. J., van Genuchten, M. T., and Gärdenäs, A. (Mar. 10, 2003). "Review and comparison of models for describing non-equilibrium and preferential flow and transport in the vadose zone". In: *Journal of Hydrology*. Soil Hydrological Properties and Processes and their Variability in Space and Time 272.1, pp. 14–35. DOI: 10.1016/S0022-1694(02)00252-4.

Steinbrich, A., Leistert, H., and Weiler, M. (Nov. 2016). "Model-based quantification of runoff generation processes at high spatial and temporal resolution". In: *Environmental Earth Sciences* 75.21, p. 1423. DOI: 10.1007/s12665-016-6234-9.

Weiler, M. (Aug. 1, 2005). "An infiltration model based on flow variability in macropores: development, sensitivity analysis and applications". In: *Journal of Hydrology* 310.1, pp. 294–315. DOI: 10.1016/j.jhydrol.2005.01.010.

Weiler, M. (Jan. 1, 2017). "Macropores and preferential flow-a love-hate relationship". In: *Hydrological Processes* 31.1, pp. 15–19. DOI: 10.1002/hyp.11074.

A Appendix

Table A.1: Representation of the event length(te-tb[h]), the maximum precipitation gap during an event [h], and the deviatoin of the modeled and observed event start[h]).

Event ID	te-tb[h]	max. Prec. gap [h]	TB-tb [h]
19025	65.0	4.5	-7.5
20606	24.5	2.0	-0.3
27769	27.7	2.0	-9.0
31213	11.2	0.7	-1.8
42651	16.3	3.3	7.8
46410	27.8	2.8	8.0
56960	44.7	4.2	17.3
62291	33.5	1.8	2.7
70968	10.7	2.0	1.7

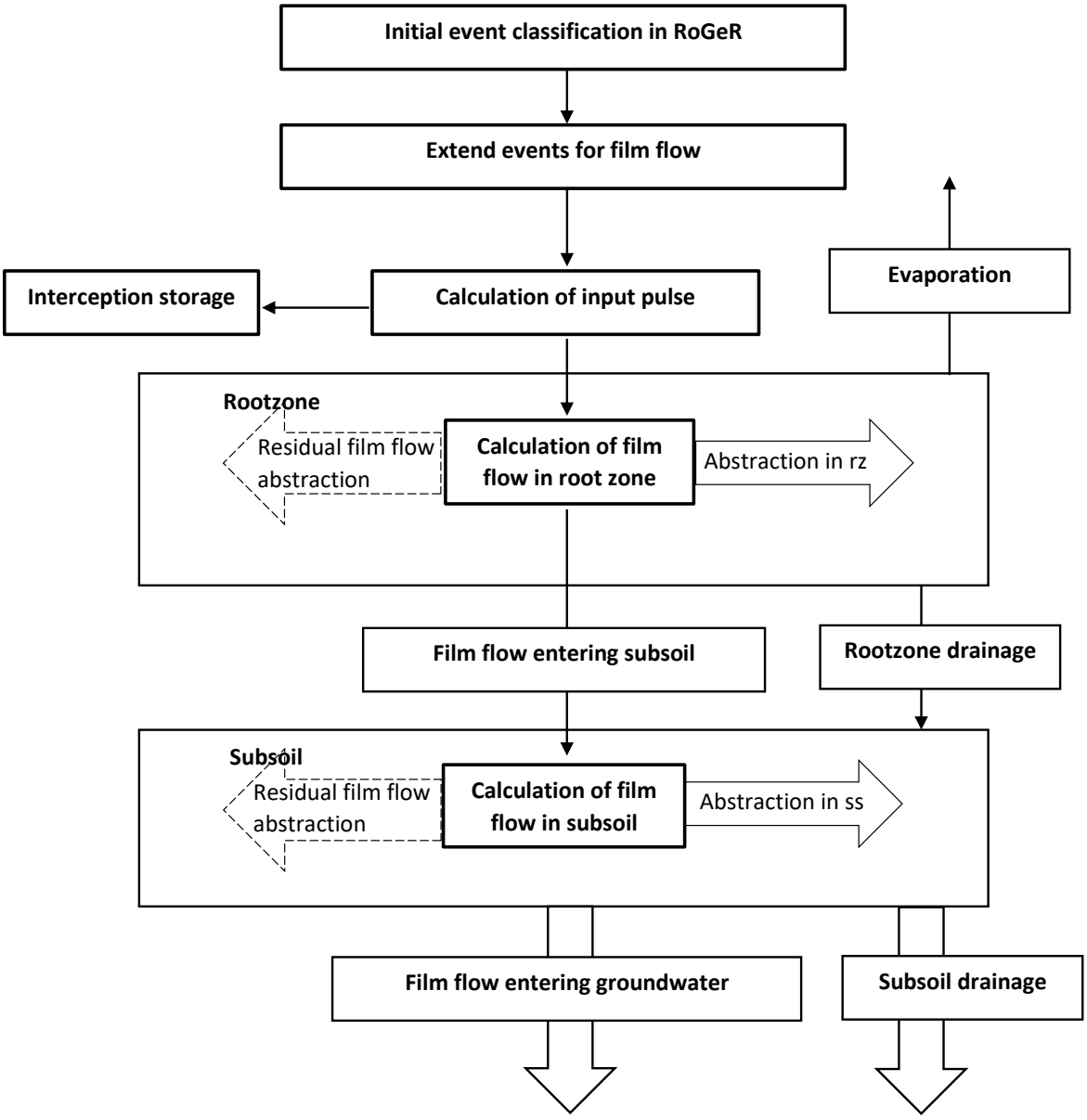

Figure A.1: A simpilifed schema of the major processes in the model. The abstraction of the residual film flow only occurs in one layer depending on the position of the wetting front.

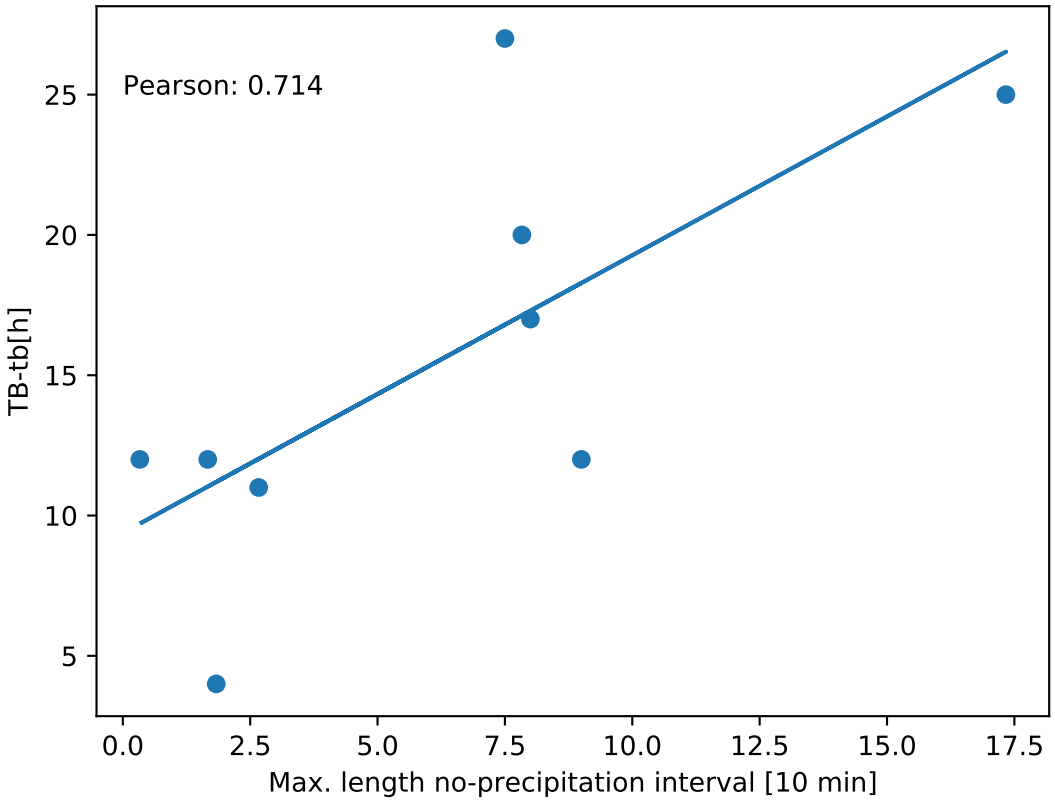

Figure A.2: Correlation between the maximum length of the non-precipitation periods and the deviation of the input pulse start point to the observed start point.